Implementation and stability analysis of prioritized whole-body compliant controllers on a wheeled humanoid robot in uneven terrains

Luis Sentis, Josh Petersen & Roland Philippsen

Autonomous Robots

ISSN 0929-5593
Volume 35
Number 4

Auton Robot (2013) 35:301-319
DOI 10.1007/s10514-013-9358-8

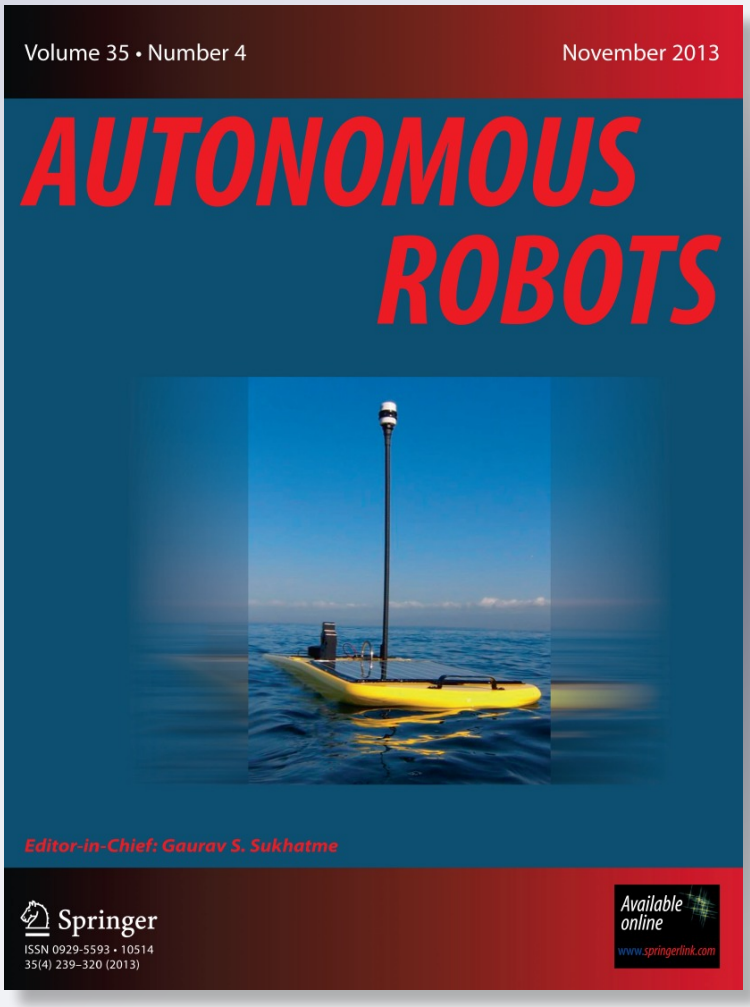

Springer

Auton Robot (2013) 35:301–319
DOI 10.1007/s10514-013-9358-8

Implementation and stability analysis of prioritized whole-body compliant controllers on a wheeled humanoid robot in uneven terrains

Luis Sentis · Josh Petersen · Roland Philippsen

Received: 12 November 2012 / Accepted: 25 July 2013 / Published online: 13 August 2013

Abstract In this work, we implement the floating base prioritized whole-body compliant control framework described in Sentis et al. (IEEE Transactions on Robotics 26(3):483–501, 2010) on a wheeled humanoid robot maneuvering in sloped terrains. We then test it for a variety of compliant whole-body behaviors including balance and kinesthetic mobility on irregular terrain, and Cartesian hand position tracking using the co-actuated (i.e. two joints are simultaneously actuated with one motor) robot's upper body. The implementation serves as a hardware proof for a variety of whole-body control concepts that had previously been developed and tested in simulation. First, behaviors of two and three priority tasks are implemented and successfully executed on the humanoid hardware. In particular, first and second priority tasks are linearized in the task space through model feedback and then controlled through task accelerations. Postures, on the other hand, are shown to be asymptotically stable when using prioritized whole-body control structures and then successfully tested in the real hardware. To cope with irregular terrains, the base is modeled as a six degree of freedom floating system and the wheels are characterized through contact and rolling constraints. Finally, center of mass balance capabilities using whole-body compliant control and kinesthetic mobility are implemented and tested in the humanoid hardware to climb terrains with various slopes.

Keywords Prioritized whole-body compliant control · Wheeled humanoid robot · Uneven terrain mobility

1 Introduction

With growing expectations on the application of humanoid robots in industries and services, future demands involve maneuvering and manipulating in irregular terrains. Examples of such environments are exterior sites such as cities, rugged manufacturing facilities, and construction sites. A common trait in these environments is the departure from a flat laboratory-like terrain to irregular or uneven surfaces. In Fig. 1, we depict a concept of utilizing those technologies in an industrial setup.

To achieve these goals, we develop here the following unique infrastructure and theoretical advancements: (1) building a new compliant humanoid robot, Dreamer, with a compliant holonomic base, (2) developing constrained models for transmission dependencies and wheel rolling contacts, (3) implementing an open source software based on the whole-body compliant control methods described in Sentis et al. (2010), (4) proving the asymptotic stability of redundant postures of floating base robots with constraints, and (5) implementing hardware tests involving kinesthetic mobility on a sloped terrain and compliant hand Cartesian tracking using the robot's co-actuated upper body.

Our line of research is a direct successor of Holmberg and Khatib (2000). Here, a mobile omnidirectional manipulator for flat terrain was developed using caster wheels and a Puma industrial manipulator which was controlled by an

Electronic supplementary material The online version of this article (doi:10.1007/s10514-013-9358-8) contains supplementary material, which is available to authorized users.

L. Sentis (✉) · J. Petersen
The University of Texas at Austin, Austin, TX, USA
e-mail: lsentis@austin.utexas.edu

J. Petersen
e-mail: joshpetersen1231@gmail.com

R. Philippsen
Halmstad University, Halmstad, Sweden
e-mail: roland.philippsen@gmx.net

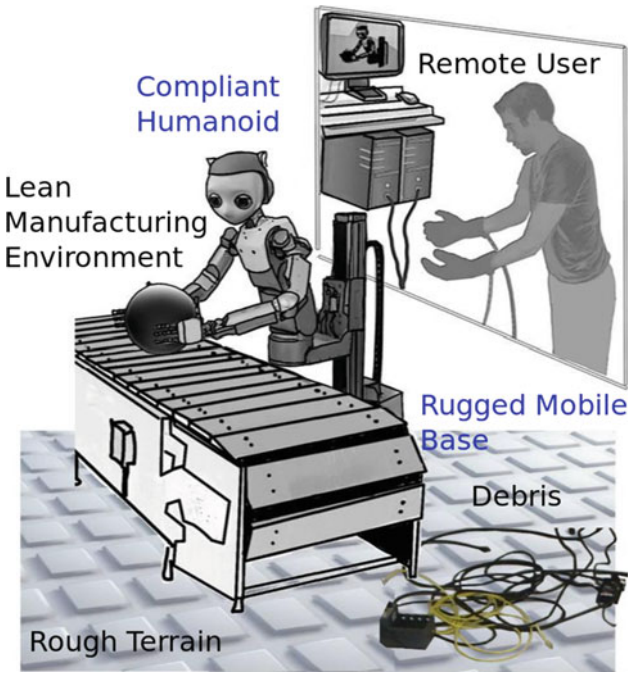

Fig. 1 *Mobile humanoid robot in rugged environment* Mobile robots with excellent mobility and dexterity will be effective in flexible manufacturing and construction environments. The illustration corresponds to our new humanoid robot Dreamer

Operational Control software (Khatib 1987). Our work is an advancement thereof in various respects: (1) we implement whole-body models that incorporate the floating base dynamics, (2) we describe the inter-dependencies between wheels as contact and rolling constraints, (3) we implement in hardware prioritized task and posture feedback controllers that ensure asymptotic stability to the minimum errors, and (4) we control balance to prevent falling in the irregular terrains. We thus provide a mobile platform that utilizes the joint redundancy more effectively and is more capable of adapting to uneven terrains while interacting with people or the environment. Whole-Body Compliant Control in mobile robots and humanoids has been thoroughly studied by our predecessors Chang et al. (2000), Brock et al. (2002) and by us Khatib et al. (2004), Sentis and Khatib (2005).

2 Related work

Recent developments in "Holistic Control Approaches" feature prominently in the body of related work. This is discussed, along with other relevant state of the art, before proceeding to the core of our contributions: (1) Real-time software implementation of the whole-body compliant control framework as described in Sentis et al. (2010), Philippsen et al. (2011), (2) a theoretical proof of asymptotic stability of redundant postures of floating base robots with constraints, (3) a new full body torque control holonomic wheeled humanoid robot for hardware testing accompanied with reconfigurable uneven terrains, and (4) rolling and contact constraints for the wheels to implement the floating base controller.

2.1 Holistic control approaches

In contrast to our foundations in Operational Space Control (Khatib 1987), an important line of work has been developed over the years focusing on simple and general solutions that rely on Inverse Dynamics (Aghili 2005). In Nakanishi et al. (2007) a torque based floating control framework that relies on estimating external contact forces to solve the constrained control problem is proposed. In Mistry et al. (2010), this work is advanced via kinematic projections that remove the need to estimate contact forces. The authors express contacts as rigid holonomic constraints and derive a QR algebraic decomposition of the constrained kinematics, with the benefit of involving only a single dynamic projection (all other operators are kinematic). In Mistry and Righetti (2011) a diversity of torque control approaches for constrained task space goals are presented and demonstrated in simulation. In Righetti et al. (2011), (2013), the authors generalize and unify the inverse dynamic control problem of floating base robot by using a projection operator that cancels constraint forces. They show that the resulting controllers can represent various derivations, including the orthogonal kinematic projections described in Mistry et al. (2010), and the operational space force projections that we presented in Sentis (2007).

In comparison to the above body of work, we rely more heavily on dynamic based operators. This increases computational complexity, but underlies a key benefit of our whole-body control methods: they provide a direct relationship between prioritized task accelerations and desired feedback control laws, which guarantees convergence to the minimum task and posture errors in case of conflicts between task goals. In particular, here we demonstrate asymptotic stability of over-determined tasks (e.g. postures or partially controllable tasks) for robustness of the whole-body controllers.

The inverse dynamics method presented in Saab et al. (2013) is another prominent example of a holistic approach. It extends previous work by the authors on inverse kinematics to inverse dynamic problems, and introduces inequality constraints and a Quadratic Program solver to obtain whole-body torques. This is currently limited to offline planning due to computational constraints, however. The work of Salini et al. (2011), (2012), is also highly relevant. They focus on a generic and recursive formulation of compliant controllers with equality and inequality const raints. This has been demonstrated in simulation only so far.

Compliant multicontact behaviors using optimal distribution of contact forces was pioneered by Hyon et al. (2007),

who focused on biped balancing and adaptation to terrain disturbances. We share many traits with this real-time torque control framework, but particularly emphasize prioritization, posture performance, and task programming. Motion planning using multicontact as described in Bouyarmane and Kheddar (2011), Lengagne et al. (2013) is also highly relevant. However, the focus of these studies is on offline planning instead of run-time torque control.

Research on holistic frameworks has recently achieved significant advances. However, a theoretical treatment its relation to whole-body operational space control is beyond the scope of this paper. Here, we present the software implementation of the methods described in Sentis (2007), (2010) on a real-world wheeled humanoid robot, and address the stability of our controllers to achieve good performance.

2.2 Related systems and setups

At the implementation level, the group of Fuchs et al. (2009), Dietrich et al. (2011) has developed a mature framework for controlling wheeled manipulators. They demonstrate impressive compliant control and application-level programming, but their work is currently limited to flat terrain and lacks active balancing. A further difference with respect to our work is their reliance on admittance control for the mobile base. Also, we have a significantly stronger focus on task conflict resolution via prioritization.

In Nagasaka et al. (2010), a constrained inverse dynamics solution based on LCP is implemented on a wheeled dual arm robot operating in a planar environment. Although the formulation is simple and elegant, the work does not give details on the implementation of prioritized tasks and it is limited to movements in planar surfaces.

A compliant omnidirectional cane robot is presented in Wakita et al. (2011). This admittance controlled device has an omnidirectional base, a six axis force sensor, a tilt angle sensor, and lasers to measure the subject's pose. Aside from the fact that the cane does not have manipulators, our work differs in that we rely on prioritized compliant torque control and contact-based constrained dynamics. As such, our framework offers more flexibility on changing the overall behaviors (i.e. it is less specific to a concrete application) and is better suited to switching or adapting to contact events.

Other wheeled humanoid robots include, Asfour et al. (2000), Beetz et al. (2010), Reiser et al. (2009), King et al. (2010), Breazeal et al. (2008), Meeussen et al. (2010), Hart et al. (2011), Iwata and Sugano (2009), Stilman et al. (2010), Katz et al. (2006), Theobold et al. (2008). Compared to our work on coordination policies at the motion and force feedback levels, they all focus more on high level sensor-based planning. These works are thus complementary and provide precise sensor-based mobility and interaction.

Like ours, the mobile system (Stilman et al. 2010) is capable of dynamically balancing, but little detail is presented on the compliant control strategy and on its ability to interact in uneven terrain.

Compliance and balancing are key capabilities of our approach. In Freitas et al. (2009), a large wheeled robot with reconfigurable pose is used to maneuver in outdoor terrains. Compared to our work, it does not utilize a flexible compliant control software which makes the vehicle application specific. A simple wheeled robot that balances in uneven roads has been proposed in Matsumoto et al. (1995). They use wheeled inverted pendulum dynamics to stabilize balance through state feedback control. This work complements a line of research on legged-wheeled robots that includes previous work by Ohmichi et al. (1985), Kimura et al. (1991), Nakano and Nagasaka (1993), Hirose et al. (1991). Although such robots are fundamentally different from ours in that they do not have manipulation capabilities, those studies complement ours.

Given our long term goal to pursue field applications, we connect with previous work that explore operations in uneven terrains, such as the legged-wheeled planetary robot described in Wilcox et al. (2007). In Halme et al. (1999), Ylonen and Halme (2002) a wheeled platform and a wheeled humanoid robot are presented for planetary operations. These previous works do not describe in detail the motor coordination policies and therefore it is impossible to draw similarities.

2.3 Software and skill architecture

We develop hardware tests based on whole-body skills from a motor control perspective. The software is an extension of the work presented in Philippsen et al. (2011) which provides structures for creating constrained behaviors online. This is enabled by means of scripting files that have access to the task and constraint parameters of the desired behaviors.

Skills, sometimes termed "behaviors" or similar variations, have often been addressed in robotics. We can distinguish top-down from bottom-up perspectives. High level skill architectures, which focus is on high level planning, include works by Volpe et al. (2001), Arkin and Murphy (1990), Alami et al. (1998), Kim et al. (2010), Simmons and Apfelbaum (1998). Data driven skills for Human Robot Interaction are explored in Jenkins and Mataric (2004). Skill encoding and control based on imitation learning can be found in Schaal et al. (2003); Pastor et al. (2009).

Compared to these works we also maintain a database of behavioral capabilities to choose from, but we do not provide a supervisory or sensor-based layer to take high level decisions. However, our skill-based architecture exploits compliance, contact and dynamics to ensure that the emergent behaviors reactively adapt to the contact environments.

3 Constraint modeling on dreamer

To characterize the robot's mobility in free space, the generalized coordinates of a wheeled robot moving in irregular terrains need to incorporate the position and orientation of the base. Thus, we express the generalized coordinates as

$$q \triangleq \left(q_{\text{freebody}} \;\; q_{\text{wheels}} \;\; q_{\text{torso}} \;\; q_{\text{arm}}\right) \in \mathbb{R}^{n_{\text{dofs}}}, \tag{1}$$

where $q_{\text{freebody}} \in SE(3)$ corresponds to the unactuated freebody position and orientation of the base, $q_{\text{wheels}} \in \mathbb{R}^3$ corresponds to the wheel actuated rolling motion, $q_{\text{torso}} \in \mathbb{R}^3$ corresponds to the robot's upper torso (including the biarticular constraint discussed below), and $q_{\text{arm}} \in \mathbb{R}^7$ corresponds to the robot's actuated right arm. Thus, $n_{\text{dofs}} = 19$.

Biarticular muscles in humans and animals correspond to muscles that attach to multiple articulations of the body. These types of dependencies are utilized for human motion analysis by biologists (Babic 2009; Oh et al. 2010) and to develop mechanical actuators that exploit reduced design complexity in humanoid robots.

Biarticular joints in Dreamer are located between the hip and the thorax segments of the torso as shown in Fig. 2. In particular, the torso has 3 degrees of freedom (DoFs) of mobility (waist rotation, hip flexion/extension, thorax flexion/extension), but only the waist rotation and the hip flexion/extension are actuated by independent motors. A steel wire runs between the hip and thorax DoFs to provide actuation to the two Sagittal joints of the upper torso. This type of transmission constraint represents a passive degree of freedom that relies on tension forces across the wire to achieve articulated movement. Because biarticular constraints create position dependencies, they are holonomic.

In particular, the biarticular constraint on the torso of Dreamer can be modeled as $q_{\text{hip}} = q_{\text{thorax}}$, where q_i corresponds to the angle of joint i. It follows that the instantaneous velocities of both joints are also equal,

$$\dot{q}_{\text{hip}} = \dot{q}_{\text{thorax}}. \tag{2}$$

Let us define the differential coordinate $\delta_{\text{biart}} \triangleq q_{\text{hip}} - q_{\text{thorax}}$. Then, using (2), a velocity relation with respect to the robot's generalized velocities can be expressed as

$$J_{\text{biart}}\, \dot{q} = 0 \tag{3}$$

where $\dot{q} \in \mathbb{R}^{n_{\text{dofs}}}$ is the vector of generalized velocities, with n_{dofs} being the total number of degrees of freedom of the robot and its free-floating base, and

$$J_{\text{biart}} \triangleq \left([0]_{1\times 6} \; [0]_{1\times 3} \; 0 \; 1 \; -1 \; [0]_{1\times 7}\right) \in \mathbb{R}^{1\times n_{\text{dofs}}}, \tag{4}$$

expressing the Jacobian of the constraint. Here the first nine zeros correspond to the free-floating base and the base wheels while the rest of the vector corresponds to the upper torso.

The relative velocity of the ground contact point of the i-th wheel, $v_{\text{contact}[i]}$, is equal to the velocity of the center of the wheel plus the cross product of the angular velocity of the wheel with the vector from the wheel's center to the contact point, i.e.

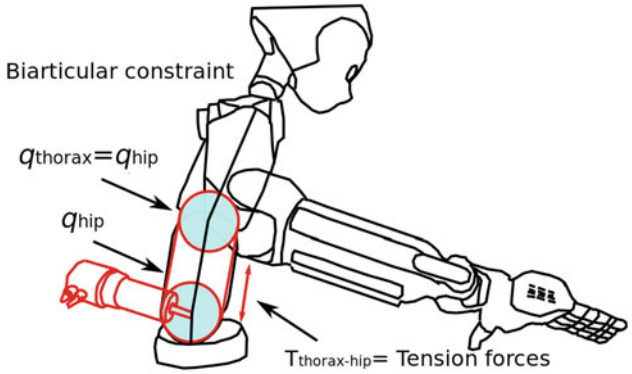

Fig. 2 *Biarticular transmission constraint* The robot's hip and thorax joints are connected with a steel wire while a single motor connected to the hip moves the two joints

$$v_{\text{contact}[i]} = v_{\text{wheel}[i]} + \omega_{\text{wheel}[i]} \times \delta_{\text{contact}[i]} \in \mathbb{R}^3, \tag{5}$$

where $v_{\text{wheel}[i]}$ and $\omega_{\text{wheel}[i]}$ are linear and angular velocities of the wheel, and $\delta_{\text{contact}[i]} \triangleq p_{\text{contact}[i]} - p_{\text{wheel}[i]}$ is the displacement between the wheel contact point and the wheel center. The rolling constraint implies that the velocity of the contact point in the direction of the wheel roll is zero, i.e.

$$u^T_{\text{rolling}[i]}\, v_{\text{contact}[i]} = 0, \tag{6}$$

where $u_{\text{rolling}[i]} \in \mathbb{R}^3$ is the direction of the wheel's axial roll. This constraint can be interpreted as the result of no slippage between the wheel and the ground in the direction of

$$J_{\text{rolling}[i]}\, \dot{q} = 0. \tag{7}$$

where

$$J_{\text{rolling}[i]} \triangleq u^T_{\text{rolling}[i]} \left(J_{\text{v,wheel}[i]} - \delta_{\text{contact}[i]} \times J_{\omega,\text{wheel}[i]}\right) \in \mathbb{R}^{1\times n_{\text{dofs}}}, \tag{8}$$

where the screw vector $\left(v^T_{\text{wheel}[i]} \; \omega^T_{\text{wheel}[i]}\right)^T = J_{\text{wheel}[i]}\, \dot{q}$ corresponds to the linear and angular velocity of the wheel, with $J_{\text{wheel}[i]} = \left(J_{\text{v,wheel}[i]} \; J_{\omega,\text{wheel}[i]}\right)^T \in \mathbb{R}^{6\times n_{\text{dofs}}}$, and $J_{\text{v,wheel}[i]}$ and $J_{\omega,\text{wheel}[i]}$ the linear and rotational parts of the wheel's basic Jacobian at the center of the wheels.

In addition to the rolling constraint, there exists a contact constraint with respect to the wheel's normal direction to the ground, i.e.

$$J_{\text{normal}[i]}\, \dot{q} = 0, \tag{9}$$

with $J_{\text{normal}[i]} \triangleq u^T_{\text{normal}[i]} J_{\text{v,wheel}}$. Therefore the combined contact constraints of the three wheels correspond to the aggregation of the rolling and the normal constraints for each wheel, i.e.

$$J_{\text{contact}} \triangleq \begin{pmatrix} J_{\text{rolling}} \\ J_{\text{normal}} \end{pmatrix} \in \mathbb{R}^{6\times n_{\text{dofs}}} \tag{10}$$

where

$$J_{\text{contact}} \triangleq \left(J^T_{\text{rolling}(1)} \cdots J^T_{\text{rolling}(3)} \; J^T_{\text{normal}(1)} \cdots J^T_{\text{normal}(3)} \right)^T. \tag{11}$$

Uniting contact and rolling constraints, we get the combined Jacobian

$$J_{\text{constr}} \triangleq \begin{pmatrix} J_{\text{biart}} \\ J_{\text{contact}} \end{pmatrix} \in \mathbb{R}^{(1+6)\times n_{\text{dofs}}}. \tag{12}$$

We finalize the modeling of Dreamer by considering its floating and co-actuated degrees of freedom. In its biarticular torso, the electrical motor is attached to the hip, and therefore the thorax joint is co-actuated. Additionally, to describe the base's inertial position and orientation we use 6 degrees of freedom which are unactuated. Overall, because there are more degrees of freedom than actuators, we consider mobile humanoids as a type of underactuated and co-actuated system. At the mathematical level, we can express underactuation / co-actuation as

$$q_{\text{act}} = U\, q, \tag{13}$$

where $q_{\text{act}} \in \mathbb{R}^{n_{\text{dofs}}-(1+6)}$ describes the actuated degrees of freedom, and

$$U \triangleq \begin{pmatrix} [0]_{3\times 6} & [I]_{3\times 3} & [0]_{3\times 3} & [0]_{3\times 7} \\ [0]_{2\times 6} & [0]_{2\times 3} & \begin{bmatrix} 1 & 0 & 0 \\ 0 & 1 & 0 \end{bmatrix} & [0]_{2\times 7} \\ [0]_{7\times 6} & [0]_{7\times 3} & [0]_{7\times 3} & [I]_{7\times 7} \end{pmatrix} \in \mathbb{R}^{\left(n_{\text{dofs}}-(1+6)\right)\times n_{\text{dofs}}} \tag{14}$$

is the matrix characterizing the actuation mapping including both the effects of the biarticular and the free-body degrees of freedom.

4 Software implementation

To conduct our tests on the new hardware, we have developed a new open source whole-body control architecture that implements the algorithms presented in our previous framework Sentis et al. (2010). We briefly present a summary of our control methods implemented into the software in Table 1. The given formulas and notation are intended to convey the essence of the algorithms implemented for our hardware tests of Sect. 6 as well as aid in following the stability proof for posture control presented in Sect. 5. More details are provided in the Appendix and our previous publications.

The software employed here includes significant additions to Philippsen et al. (2011) while adhering to the same objectives: (1) separation of concerns into mathematical foundations, run-time configurability, and independence from specific implementation environments; (2) support for two types of end-users, namely control integrators and researchers; and (3) support for experimentation and system integration, via data logging, parameter reflection, and interactive online configuration. The software relies on widespread open-source libraries, while avoid undue dependencies on any particular middleware or operating system.

Figure 3 depicts the main software components and the information they exchange during operation. The Controller implements Algorithm 1 to compute the torque commands τ_{motors}, based on the constraint consistent Jacobians J_i^* and the desired acceleration commands u_i. The latter are provided by the Task objects in the currently active task hierarchy. Truncated singular-value decomposition (SVD) is used for computing pseudo inverses and denoted $(\cdot)^+$. SVD thresholds can be configured separately for each task. The Model estimates the whole-body floating base kinematics and dynamics, used by tasks for internal updates and by the controller for gravity compensation and dynamic decoupling. The active Skill determines the task hierarchy, which is termed "current state" in Fig. 3 as it relies on a finite-state machine to processes external information as well as internal task feasibility signals. The system architecture diagram hints at the run-time configurability and reflection capabilities by indicating parameter lists associated with the skill, tasks, and the controller. These parameters are declared in the source code and can be enumerated and changed at run-time.

In our extension of this software to underactuated and constrained robots, we implement model constraints and the floating base controller following the design objectives of the original version. Constraints are independent of the robot and are run-time re-configurable allowing simple reuse and extensibility. As many constraints such as contact or rolling require only information about their location and orientation relative to the robot's body, a library of generalized constraints was created to support users focused on control applications. In addition, although not demonstrated here, the ability to change constraints during run-time was included to create more complex behaviors such as wheels losing contact with the ground when going over very rough terrain.

5 Stability of postures

To follow the proof presented in this section, the reader can refer to the notation of whole-body control summarized in Table 1 or our previous work Sentis et al. (2010) as summarized in the Appendix.

Posture control of redundant manipulators has been thoroughly analyzed in the context of inverse kinematic control (Hanafusa et al. 1981; Nakamura et al. 1987; Siciliano and Slotine 1991; DeLuca 1991; Oriolo 1994; Baerlocher 2001).

Table 1 *Summary of prioritized whole-body compliant control* detailed descriptions can be found in the Appendix

Summary of prioritized whole-body compliant control	
Constrained dynamics	
$q_{\text{act}} \in \mathbb{R}^{n_{\text{dofs}}-(1+6)}$	Actuated degrees of freedom
$q_{\text{act}} = U\, q$	Mapping between generalized and actuated positions
$U \in \mathbb{R}^{\left(n_{\text{dofs}}-(1+6)\right)\times n_{\text{dofs}}}$	Actuation / co-actuation matrix
$J_{\text{constr}} \triangleq \begin{pmatrix} J_{\text{biart}} \\ J_{\text{contact}} \end{pmatrix} \in \mathbb{R}^{(1+6)\times n_{\text{dofs}}}$	Constrained Jacobian
$N_{\text{constr}} \triangleq I - \overline{J}_{\text{constr}} J_{\text{constr}}$	Dynamically consistent null space of J_{constr}
$A\,\ddot{q} + N_{\text{constr}}^T\,(b+g)$ $+J_{\text{constr}}^T \Lambda_{\text{constr}} \dot{J}_{\text{constr}} \dot{q} = (U\,N_{\text{constr}})^T\,\tau_{\text{control}}$	Constrained floating rigid body dynamics
Prioritized task control	
$\dot{x}_{\text{task}(k)} = J^*_{\text{task}(k)}\,\dot{q}_{\text{act}}$	Constraint consistent differential task kinematics with priority k
$J^*_{\text{task}(k)} \triangleq J_{\text{task}(k)} \overline{UN}_{\text{constr}} N^*_{\text{prec}(k)}$	Reduced constraint consistent task Jacobian with priority k
$N^*_{\text{prec}(k)} \triangleq I - \sum_{i=1}^{k-1} \overline{J}^*_{\text{task}(i)} J^*_{\text{task}(i)}$	Dynamically consistent null space of higher priority tasks
$\tau_{\text{control}} = J^{*T}_{\text{task}(k)} F_{\text{task}(k)}$	Operational space torque control structure
$\Lambda^*_{\text{task}(k)} \ddot{x}_{\text{task}(k)} + \mu^*_{\text{task}(k)} + p^*_{\text{task}(k)} = F_{\text{task}(k)}$	Equation of motion in task space
$F_{\text{task}(k)} = \Lambda^*_{\text{task}(k)} u_{\text{task}(k)} + \mu^*_{\text{task}(k)} + p^*_{\text{task}(k)}$	Feedback linearization of prioritized tasks
$\ddot{x}_{\text{task}(k)} = u_{\text{task}(k)}$	Closed loop whole-body control linearized dynamics
Posture control	
$\tau_{p\|t} = J^{*T}_{p\|t} F_{\text{posture}}$	Posture space torque control structure
$\ddot{q}_{\text{act}} + \phi^*\,(b^* + g^*) = \phi^*_{p\|t} F_{\text{posture}}$	Equation of motion in posture space
$F_{\text{posture}} = \left(\phi^*_{p\|t}\right)^+ v + \left(\phi^*_{p\|t}\right)^+ \phi^*\,(b^* + g^*)$	Feedback linearization of postures
$\left(U^{\text{rank}}_{p\|t}\right)^T \ddot{q}_{\text{act}} = \left(U^{\text{rank}}_{p\|t}\right)^T v$	Closed loop dynamics of over-determined postures.
$U^{\text{rank}}_{p\|t} \in \mathbb{R}^{n_{\text{act}}\times(n_{\text{act}}-n_{\text{task}})}$	Set of controllable vectors in posture space

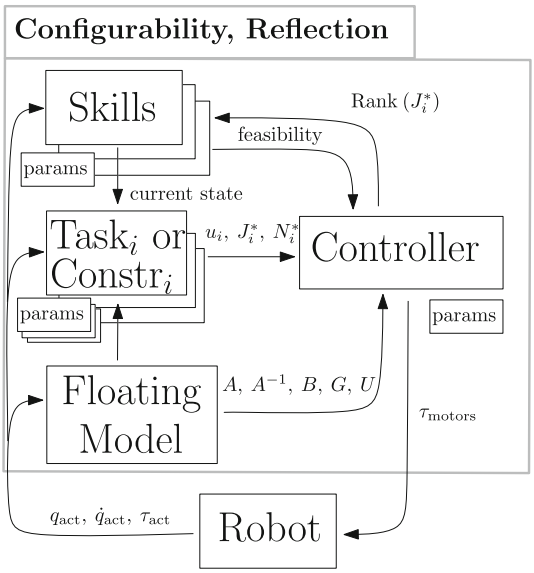

Fig. 3 Architectural overview of the whole-body control software

Algorithm 1 Hierarchical Task Decomposition

Input:
joint-space inverse inertia matrix A^{-1}
joint-space gravity torque vector G
desired task accelerations u_i
prioritize task Jacobians J_i^*
null space of constraints N_c
actuation matrix U
Output:
motor torque vector τ_{motors}
Recursion:
$\tau_{\text{motors}} \leftarrow 0$
$N^*_{(-1)} \leftarrow I$
for all $0 \le i <$ numTasks **do**
$J_i^* \leftarrow J_i \overline{UN}_c N^*_{i-1}$
$\Lambda_i^* \leftarrow \left(J_i^* A^{-1} J_i^{*T}\right)^+$
$p_i^* \leftarrow \Lambda_i^* J_i^* A^{-1} G$
$u_i \leftarrow \begin{cases} \text{State Feedback Control,} \\ \quad \text{PID Control,} \\ \quad\quad \text{Other...} \end{cases}$ ▷ Control Law
$\tau_i \leftarrow \tau_{i-1} + J_i^{*T}\left(\Lambda_i^* u_i + \mu_i^* + p_i^*\right)$
$N_i^* \leftarrow I - \sum_{k=1}^{i-1} \overline{J}_k^* J_k^*$
end for
$\tau_{\text{motors}} \leftarrow \tau_{\text{numTasks}}$

More recently, it has been studied by us in the context of compliant control (Khatib et al. 2004; Sentis 2007). However, convergence to the minimum postural energy has not been demonstrated before, aside from the conference version of this paper Sentis et al. (2012). When we started to control Dreamer, we were compelled to demonstrate the convergence properties to ensure robust and stable performance. The study here reflects these derivations.

We will often refer to the whole-body equations summarized in the Appendix. Let us focus on the part of Eq. (86) that deals with the posture. Uncontrolled null-space postures are known to produce unstable behaviors (DeLuca 1991). Therefore, we investigate the stabilizing properties of feedback controllers for the posture. We consider the following energy function to be minimized in posture space

$$V_{\text{posture}} = \frac{1}{2} e_{\text{act}}^T k_p \, e_{\text{act}}, \tag{15}$$

where

$$e_{\text{act}} \triangleq q_{\text{act}} - q_{\text{act}}^{\text{goal}} \tag{16}$$

is a feedback error function, $q_{\text{act}}^{\text{goal}}$ is a desired postural attractor goal and k_p is a proportional gain multiplier. A common approach is to project the gradient of (15) plus a damping term directly into the control structure (86), i.e.

$$\tau_{\text{control}} = J_{\text{task}}^{*T} F_{\text{task}} + N_{\text{task}}^{*T} \left(-k_p e_{\text{act}} - k_v \dot{q}_{\text{act}} \right), \tag{17}$$

where k_v is a damping gain. If we apply the above torque to the posture dynamics (which in our example are equal to the actuated dynamics) of Eq. (78), and neglect the task torques, i.e. $F_{\text{task}} = 0$, we get

$$\ddot{q}_{\text{act}} + \phi^* \, N_{\text{task}}^{*T} \left(k_p e_{\text{act}} + k_v \dot{q}_{\text{act}} \right) + \phi^* \left(b^* + g^* \right) = 0. \tag{18}$$

The problem with this policy, besides the lack of compensating for gravity and Coriolis/centrifugal terms, is that if the gradient of the energy falls under the condition

$$k_p e_{\text{act}} \in \text{Null} \left(N_{\text{task}}^{*T} \right), \tag{19}$$

then convergence to the minimum achievable energy may not be possible. This type of deficiency was first studied by Oriolo (1994) who stated that the joint error e_{act} gets "stuck" in the null space of N_{task}^{*T}. They proposed a solution based on a feedback stabilization scheme where the gain k_p changes in a time-varying cyclical fashion. This solution was carefully designed for a simple 3 DoF robot and in the context of velocity control, with no proposal for extensions to systems with many degrees of freedom or controlled through compliant structures.

An initial study of feedback control policies to mitigate this problem in the context of compliant control for humanoid robots was conducted in Khatib et al. (2004). However, a proof of stability and convergence of the self motions in the context of the proposed compliant controllers has been newly conducted first in Sentis et al. (2012) and then improved and extended for this journal manuscript.

In Khatib et al. (2004), we investigated this problem in the context of dynamic behavior of postural control, and proposed an initial control strategy for compliant postures. It was found that the following control structure has linearizing properties,

$$\tau_{p|t} = J_{p|t}^{*T} F_{\text{posture}}, \tag{20}$$

where $\tau_{p|t} \triangleq N_{\text{task}}^{*T} \tau_{\text{posture}}$ is the right-most term of (86),

$$J_{p|t}^* \triangleq J_{\text{posture}}^* N_{\text{task}}^*, \tag{21}$$

is the task consistent posture Jacobian matrix and the matrix $J_{\text{posture}}^* \triangleq U \, \overline{UN}_{\text{constr}}$, is the reduced constraint consistent Jacobian of the posture. Notice that, for this paper we consider a posture coordinate that attempts to control all actuated joints defined as $q_{\text{act}} = U \, q$.

Let us study in detail the stability of the self-motions. If we plug (20) into (78) we get

$$\ddot{q}_{\text{act}} + \phi^* \left(b + g \right) = \phi^* J_{p|t}^{*T} F_{\text{posture}}. \tag{22}$$

In Sentis (2007) we defined the pseudo inertial matrix

$$\phi_{p|t}^* \triangleq \phi^* J_{p|t}^{*T}, \tag{23}$$

which allows us to rewrite the closed loop dynamics associated with Eq. (22) as

$$\ddot{q}_{\text{act}} + \phi^* \left(b^* + g^* \right) = \phi_{p|t}^* F_{\text{posture}}. \tag{24}$$

Defining the general controller

$$F_{\text{posture}} = \left(\phi_{p|t}^* \right)^+ v + \left(\phi_{p|t}^* \right)^+ \phi^* \left(b^* + g^* \right) \tag{25}$$

yields the closed loop behavior (Sentis 2007)

$$\ddot{q}_{\text{act}} = \Phi_{p|t}^* \, v, \tag{26}$$

where v is a user-defined feedback control policy and

$$\Phi_{p|t}^* \triangleq \phi_{p|t}^* \, \phi_{p|t}^{*+}. \tag{27}$$

We can further explore the structure of $\Phi_{p|t}^*$ if we consider the following minimal (rank) Singular Value Decomposition

$$\phi_{p|t}^* = U_{p|t}^{\text{rank}} \, \Sigma_{p|t}^{\text{rank}} \left(U_{p|t}^{\text{rank}} \right)^T, \tag{28}$$

where

$$U_{p|t}^{\text{rank}} \in \mathbb{R}^{n_{\text{act}} \times (n_{\text{act}} - n_{\text{task}})}, \tag{29}$$

is the set of controllable eigenvectors of $\phi_{p|t}^*$. Using orthogonal properties of the Singular Value Decomposition of Eq. (28), we can express Eq. (27) as

$$\Phi_{p|t}^* = U_{p|t}^{\text{rank}} \left(U_{p|t}^{\text{rank}} \right)^T, \tag{30}$$

and therefore it follows that the above matrix is singular and symmetric positive semidefinite. Additionally, by using the property derived from the Singular Value Decomposition,

$$\left(U_{p|t}^{\text{rank}}\right)^T U_{p|t}^{\text{rank}} = I, \tag{31}$$

and given the expression of $\Phi_{p|t}^*$ given in Eq. (30), left multiplying Eq. (26) by $(U_{p|t}^{\text{rank}})^T$ yields

$$\left(U_{p|t}^{\text{rank}}\right)^T \ddot{q}_{\text{act}} = \left(U_{p|t}^{\text{rank}}\right)^T v. \tag{32}$$

In other words, our control structures project the unconstrained closed-loop dynamics ($\ddot{q}_{\text{act}} = v$) into a reduced space of controllable motions that is consistent with the task constraints.

We consider again the posture error e_{act} defined in Eq. (16). Our objective is to design a control policy v that yields asymptotic stability toward the minimum possible posture error while being consistent with tasks and constraints. The best possible error that we can nullify is the full posture error projected onto the controllable directions, defined by the pseudo-coordinates

$$e_\xi \triangleq \left(U_{p|t}^{\text{rank}}\right)^T e_{\text{act}}. \tag{33}$$

To derive the error dynamics, we double differentiate the above expression to yield

$$\ddot{e}_\xi \triangleq \left(U_{p|t}^{\text{rank}}\right)^T \ddot{q}_{\text{act}} + 2\left(\dot{U}_{p|t}^{\text{rank}}\right)^T \dot{q}_{\text{act}} + \left(\ddot{U}_{p|t}^{\text{rank}}\right)^T e_{\text{act}}. \tag{34}$$

Isolating the term $\left(U_{p|t}^{\text{rank}}\right)^T \ddot{q}_{\text{act}}$ from above and plugging it in Eq. (32) we get

$$\ddot{e}_\xi = \left(U_{p|t}^{\text{rank}}\right)^T v + 2\left(\dot{U}_{p|t}^{\text{rank}}\right)^T \dot{q}_{\text{act}} + \left(\ddot{U}_{p|t}^{\text{rank}}\right)^T e_{\text{act}}. \tag{35}$$

To linearize the above closed loop dynamics, let us consider the control vector

$$v = U_{p|t}^{\text{rank}} v' - 2U_{p|t}^{\text{rank}}\left(\dot{U}_{p|t}^{\text{rank}}\right)^T \dot{q}_{\text{act}} - U_{p|t}^{\text{rank}}\left(\ddot{U}_{p|t}^{\text{rank}}\right)^T e_{\text{act}}. \tag{36}$$

Substituting v into Eq. (35) and using again the property of Eq. (31), leads to the closed-loop linear system

$$\ddot{e}_\xi = v'. \tag{37}$$

The choice of a simple proportional-derivative feedback control policy

$$v' = -k_p e_\xi - k_v \dot{e}_\xi, \tag{38}$$

will render global asymptotic stability of Eq. (37) to the equilibrium point $e_\xi = \dot{e}_\xi = 0$, demonstrating convergence to the minimum achievable postural energy.

Combining (36) and (38) and plugging the result into the force command (25) we derive the following dynamically weighted feedback control policy which eliminates the usage of the reduced coordinates e_ξ,

$$F_{\text{posture}} = \left(\phi_{p|t}^*\right)^+ \left[-k_p e_{\text{act}} - k_v \dot{q}\right] + \left(\phi_{p|t}^*\right)^+ \phi^* \left(b^* + g^*\right) - k_v \left(\phi_{p|t}^*\right)^+ U_{p|t}^{\text{rank}} \left[\left(U_{p|t}^{\text{rank}}\right)^T \dot{q}_{\text{act}} + \left(\dot{U}_{p|t}^{\text{rank}}\right)^T e_{\text{act}}\right], \tag{39}$$

where we have used the definition of the reduced coordinates given in Eq. (33), the decomposition of the inertial weighting factor $\Phi_{p|t}^*$ given in Eqs. (30) and (27), and the general property of generalized inverses, $\phi_{p|t}^{*+}\phi_{p|t}^*\phi_{p|t}^{*+} = \phi_{p|t}^{*+}$. A controller of this form is relatively easy to implement and suitable for real-time operation when it relies on a fast rigid body dynamic solver such as Featherstone (1987).

6 Hardware tests

Dreamer, our mobile dexterous humanoid robot, consists of a torso-arm-hand system with series elastic actuators, built by Meka Robotics (Edsinger and Kemp 2008), mounted on a current-controlled holonomic base designed and built by us (with electronics provided by Meka Robotics). The actuators for the upper body contain torque sensors that allow active torque feedback control. The holonomic base contains an inertial measurement unit (IMU) whose location is highlighted in Fig. 4. The base achieves holonomic motion by utilizing Omni wheels located in an equilateral triangular.

The objective of the experiments is to perform an initial assessment of various capabilities: (1) that we can run our whole-body torque controller for the 19 DoF floating system at real-time rates, including the various constraints and tasks; (2) that the robot can transition safely (i.e. without falling) between flat and the sloped portions of the terrains, at a range of speeds; (3) that the IMU and the constrained models are effectively used to perform odometry and to update the models and feedback controllers; (4) that the robot can balance in response to human disturbances; (5) that posture energies converge to their minimum (i.e. asymptotic stability) given the center of mass and hand control priority tasks; and (6) that all desired objectives can be accomplished while complying with the biarticular transmission constraints of the upper body.

Since our control framework is based on dynamic operators, we have developed models of Dreamer. We have first used CAD models of the robot's upper body, provided by Meka Robotics as well as models of the actuators' rotor inertias and harmonic drive gear ratios. We determined the mass of the base both from CAD models and using a scale. The position of the center of mass of the base was estimated using the CAD model.

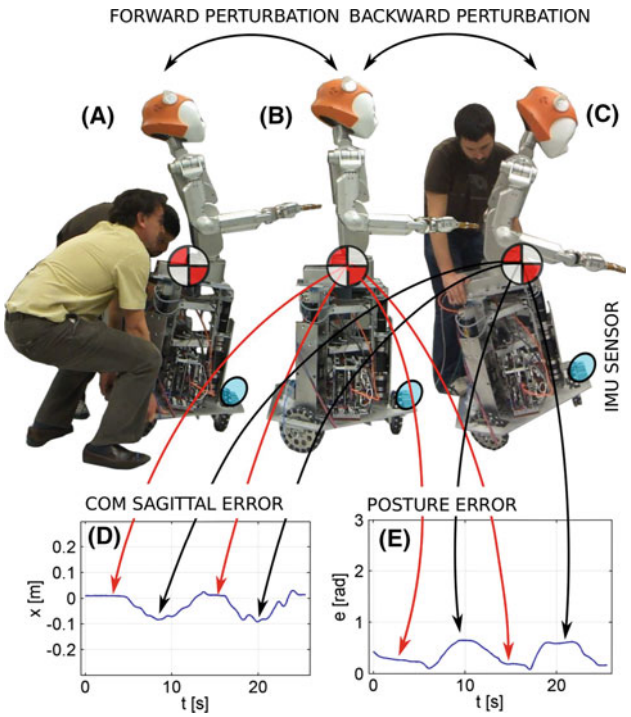

Fig. 4 *Test on balancing* Using a balance controller that relies on tilt sensing feedback (based on an inertial measurement unit (IMU) sensor as shown in the pictures), we demonstrate the ability of the robot to adapt to balance perturbations by adjusting its center of mass over the center of the wheels in the horizontal plane. The disturbances are about $\pm 30°$. The sequence **a** and **b** depicts adaptation to forward perturbations, while the sequence **b** and **c** shows adaptation to backward tilts. The data on **d** shows a maximum dynamic error of the center of mass during the perturbation **b** and **c** of 8 cm while the data on **e** shows that the whole-body controller (not described here) is able to keep the postural error low. Without a balance controller, the maximum swing of the center of mass would be around 25 cm

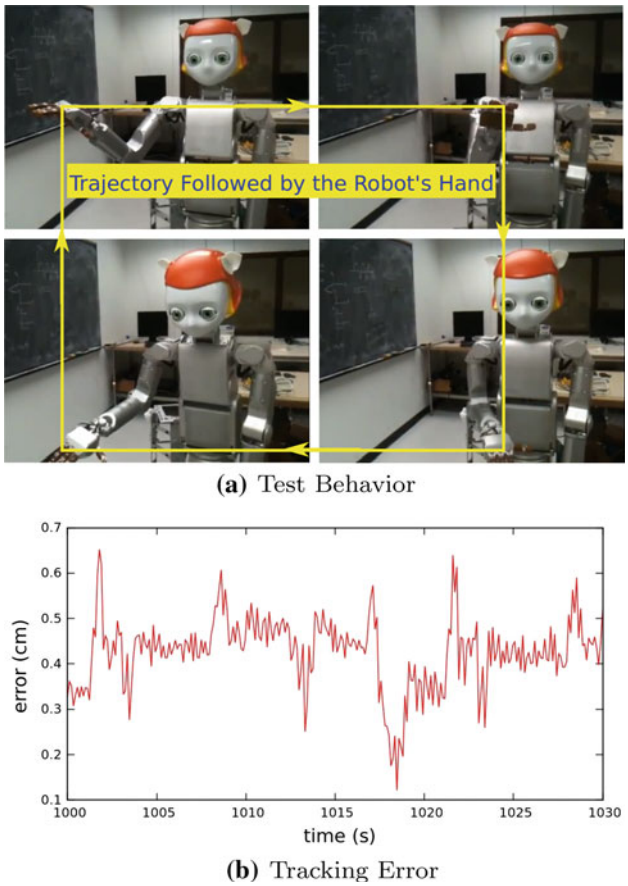

Fig. 5 *Accuracy/precision performance of dreamer's operational hand task using whole-body torque control* A Proportional-Derivative feedback control law is implemented with proportional gain equal to $K_p = 160$ N/m and derivative gain of $k_d = \eta 2\sqrt{k_p}$, where $0 < \eta < 1$ is a parameter that we tune for the experiment. For this experiment, whole-body torque control is implemented for the upper body, including the biarticular constraints. At the servo level, Dreamer employs torque-velocity feedback control as explained in Vallery et al. (2007). The current accuracy shown here is around 5 mm

As an initial validation of whole-body torque control tracking, we conducted accuracy tests on Dreamer's upper body as shown in Fig. 5. The hand compliantly tracks a rectangular trajectory with an accuracy of 5 mm for a proportional gain of 160 N/m.

Figure 6 shows the test setup for investigating the handling of irregular terrain while physically interacting with a human user. This type of skill is difficult to achieve, because the robot needs to actively balance on the terrain while executing the compliant interaction with the human. For the test, two large wooden boards are used, one measuring 1.8×1 m^2 lying flat on the ground and another one measuring 1.2×1.2 m^2 sloping up from the lab's floor through a supporting stud. The slope is 7° at first and increased to 16° in later tests. Sandpaper sheets were glued to the wooden boards, to prevent wheel slippage on the slope, but at 16° the provided friction started to be insufficient.

To show the desired capabilities, we create a skill for interacting with a human user in the irregular terrain. In particular, to prevent the robot from falling down when transitioning from flat to sloped terrain, we define an active balance task based on center of mass coordinates in the horizontal plane, $x_{\text{com}} \in \mathbb{R}^2$. To demonstrate that the robot can respond compliantly to physical interactions with a human user, we define a compliant position frame on the robot's hand with respect to the robot's base frame, i.e. $(x_{\text{hand}} - x_{\text{base}}) \in \mathbb{R}^3$. To stabilize the self-motion and converge to a human-like posture, we define postural coordinates, $x_{\text{posture}} = \text{subset}(q_{\text{act}})$. The whole-body skill in the irregular terrain thus takes the form

$$x_{\text{skill}}(q) \triangleq \begin{Bmatrix} x_{\text{com}} \\ (x_{\text{hand}} - x_{\text{base}}) \\ x_{\text{posture}} \end{Bmatrix} \in \mathbb{R}^{2+3+n_{\text{posture}}}. \tag{40}$$

We now characterize the kinematics of the various tasks of the skill (40). For balance, we choose the coordinate description

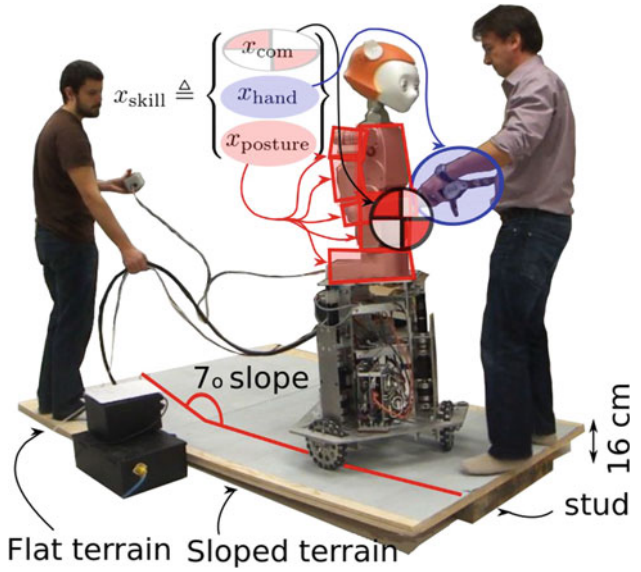

Fig. 6 *Skill for uneven terrain interaction* A skill formed with three coordinates, namely CoM, hand-base relative Cartesian position, and joint posture, is used to kinesthetically interact with the robot on the uneven terrain

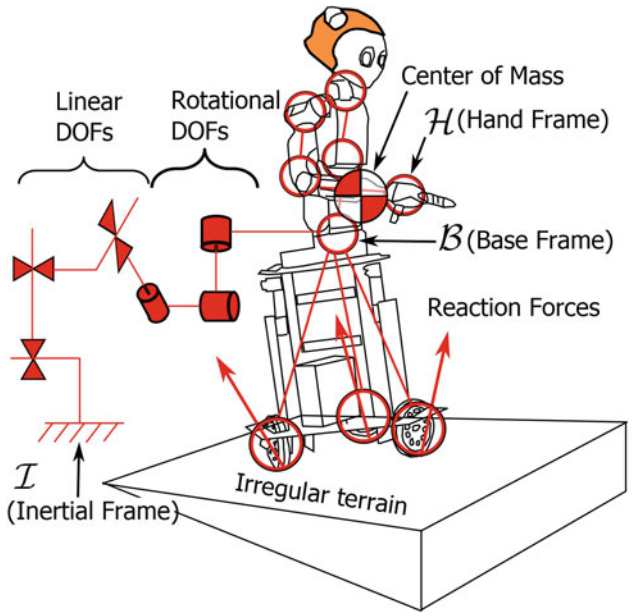

Fig. 7 *Floating-body underactuated/co-actuated contact dynamics* In order to adapt to irregular terrains, we model the robot kinematics and dynamics with respect to an inertial reference frame. This step entails adding 6 kinematic degrees of freedom of floating-body movement to the kinematic description of the robot as well as considering rolling and contact constraints on the wheels

$$x_{\text{com}} \triangleq \frac{1}{M} \sum_{i=i_{\text{base}}}^{n_{\text{dofs}}} m_i \, x_{\text{com}[i]} \tag{41}$$

where M is the total mass of the robot, $i_{\text{base}} = n_{\text{freebody}} + n_{\text{wheels}}$ is the first joint attached to the upper body base in the kinematic chain depicted in Fig. 7. The center of mass Jacobian can be described as

$$J_{\text{com}}(q) = \frac{1}{M} \sum_{i=i_{\text{base}}}^{n_{\text{dofs}}} m_i \, J_{\text{com}[i]}(q), \tag{42}$$

where $J_{\text{com}[i]}$ is the Jacobian of the i-th linkage in the kinematic chain. The hand coordinate system can be derived from the homogeneous transformation from the Inertial Frame, $\mathcal{I}$, to the Hand Frame, $\mathcal{H}$, both depicted in Fig. 7. We can represent the hand frame as

$$\begin{pmatrix} x_{\text{hand}} - x_{\text{base}} \\ 1 \end{pmatrix} = \prod_{i=0}^{n_{\text{hand}}} {}^{i+1}T_i(q) \begin{pmatrix} {}^{\mathcal{H}}x_{\text{hand}} \\ 1 \end{pmatrix} \tag{43}$$

$$- \prod_{i=0}^{n_{\text{base}}} {}^{i+1}T_i(q) \begin{pmatrix} {}^{\mathcal{B}}x_{\text{base}} \\ 1 \end{pmatrix}, \tag{44}$$

where $(x_{\text{hand}} - x_{\text{base}})$ is the vector of relative hand-base translations with respect to the inertial frame $\mathcal{I}$, ${}^{i+1}T_i(q)$ is the matrix describing the Homogeneous Transformation from frame $i+1$ to frame i, ${}^{\mathcal{H}}x_{\text{hand}}$ is the hand translation expressed in its local frame $\mathcal{H}$, and ${}^{\mathcal{B}}x_{\text{base}}$ is the base translation expressed in its local frame $\mathcal{B}$. The Jacobian of the hand-base frame is the geometric operator

$$J_{\text{hand-base}}(q) \triangleq \frac{\partial x_{\text{hand}}}{\partial q} - \frac{\partial x_{\text{base}}}{\partial q}. \tag{45}$$

The posture coordinates correspond to actuated joints of the upper body. The wheel angles of rotation are not included as part of the posture. Therefore, we describe the posture coordinate as

$$x_{\text{posture}} = S_{\text{act}}^{\text{upper}} \, q, \tag{46}$$

where $S_{\text{act}}^{\text{upper}}$ is a selection matrix corresponding to the actuated joints of the upper body only. It follows that the posture Jacobian is $J_{\text{posture}} = S_{\text{act}}^{\text{upper}}$.

We propose to use the prioritized whole-body compliant controller summarized on Table 1 to endow the desired skill to the mobile humanoid. Using notation similar to Sentis et al. (2010), we use the following control structure to accomplish the desired motor skill,

$$\tau_{\text{control}} = J_{\text{com}}^{*T} F_{\text{com}} + J_{\text{hb}}^{*T} F_{\text{hb}} + J_{\text{posture}}^{*T} F_{\text{posture}}, \tag{47}$$

where a priority structure is enforced by projecting tasks on the right hand side into the null space of the tasks on the left hand side. Notice that we have used the abbreviation "hb" to denote "hand-base". As such, the center of mass operates with higher priority than the hand task and the hand task operates with higher priority than the posture task, i.e.

$$\text{com} > \text{hb} > \text{posture}. \tag{48}$$

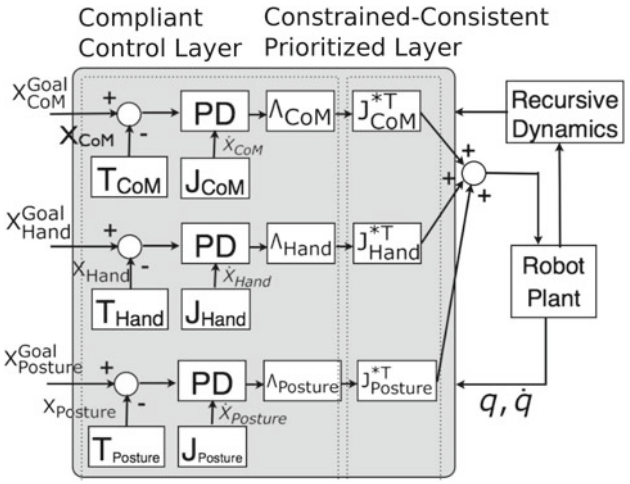

Fig. 8 *Prioritized whole-body compliant controller for dreamer* Shown here is the controller used for the tests in the irregular terrains (see Fig. 9)

In our interpretation, priorities are enforced by recursively defining the differential manifold of the self-motion of higher priority tasks, i.e.

$$J^*_{\text{com}} = J_{\text{com}}\overline{UN}_{\text{constr}}, \tag{49}$$

$$J^*_{\text{hb}} = J_{\text{hb}}\overline{UN}_{\text{constr}}N^*_{\text{com}}, \tag{50}$$

$$J^*_{\text{posture}} = J_{\text{posture}}\overline{UN}_{\text{constr}}N^*_{\text{hand,com}}, \tag{51}$$

with the null spaces of self-motion expressed as Sentis (2007)

$$N^*_{\text{com}} = I - \overline{J}^*_{\text{com}}J^*_{\text{com}}, \tag{52}$$

$$N^*_{\text{hb,com}} = I - \overline{J}^*_{\text{hb}}J^*_{\text{hb}} - \overline{J}^*_{\text{com}}J^*_{\text{com}}. \tag{53}$$

The above control structures take advantage of the models for irregular terrains and the constraints developed in Sect. 4 to achieve dynamic consistency. F_{com}, F_{hb}, and F_{posture} constitute the task-level feedback control policies. In particular, the goals of the task coordinates are the following: (1) to move the robot's center of mass to a goal position located at the center of the triangle defined by the horizontal projection of the wheels (see Fig. 8); (2) to maintain a user defined relative hand-base distance; compliance of this frame to user force disturbances is accomplished by reducing the gain of the controller; (3) to steer the upper body joint posture to the zero initial pose, except for the elbow joint which is commanded to move to the 90° bent position. These goals can be summarized as follows,

$$x^{\text{goal}}_{\text{com}} = \text{horizontal projection center of wheels} \in \mathbb{R}^2 \tag{54}$$

$$x^{\text{goal}}_{\text{hb}} = \text{predefined hand-base distance} \in \mathbb{R}^3 \tag{55}$$

$$x^{\text{goal}}_{\text{posture}} = \text{zero posture with elbow bent} \in \mathbb{R}^{n_{upperbody}-1}. \tag{56}$$

In particular, notice that by commanding the center of mass to move to the center of the wheels, we ensure that the robot balances on the moving base and not on a global fixed position. Also, notice that because we control the relative distance between the hand and the base, when the hand is perturbed by external forces, both the hand and the base will push in opposite directions to minimize the distance. As a result, when the user keeps pushing the hand, the base will follow the user in an attempt to minimize the hand-base distance. This is how the kinesthetic mobility effect appears.

We assume that the center of mass and hand tasks are non-singular in their priority spaces, therefore, the objectives of these tasks are to asymptotically converge to the goals. The proposed dynamically weighted feedback control policies for the two operational tasks and the posture are

$$F_{\text{com}} = \Lambda^*_{\text{com}}\left(-k_{p,\text{com}}\, e^{\text{goal}}_{\text{com}} - k_{v,\text{com}}\,\dot{x}_{\text{com}}\right) + p^*_{\text{com}}, \tag{57}$$

$$F_{\text{hb}} = \Lambda^*_{\text{hb}}\left(-K_{p,\text{hb}}\, e^{\text{goal}}_{\text{hb}} - K_{v,\text{hb}}\,\dot{x}_{\text{hb}}\right) + p^*_{\text{hb}},$$

$$F_{\text{posture}} = \Lambda^*_{\text{posture}}\left(-k_{p,\text{posture}}\, e^{\text{goal}}_{\text{posture}} - k_{v,\text{posture}}\,\dot{x}_{\text{posture}}\right) + p^*_{\text{posture}}, \tag{58}$$

where $\{\Lambda^*_i,\ p^*_i\}$ correspond to inertial weighting and gravity compensation operators in the operational space, as described in Sentis (2007). In particular the postural inertial weighting above corresponds to that defined in Eq. (39), i.e. $\Lambda^*_{\text{posture}} \triangleq (\phi^*_{p|t})^+$.

Given the above linearizing control laws, the resulting closed-loop dynamics of the task coordinates become

$$\ddot{x}_{\text{com}} + k_{p,\text{com}}e^{\text{goal}}_{\text{com}} + k_{v,\text{com}}\dot{x}_{\text{com}} = 0, \tag{59}$$

$$\ddot{x}_{\text{hb}} + K_{p,\text{hb}}e^{\text{goal}}_{\text{hb}} + K_{v,\text{hb}}\dot{x}_{\text{hb}} = 0, \tag{60}$$

which are asymptotically stable to the goals, while the closed-loop dynamics of the posture, according to Eq. (32) becomes

$$U^T_{\text{r,posture}}\left(\ddot{x}_{\text{posture}} + k_{p,\text{posture}}e^{\text{goal}}_{\text{posture}} + k_{v,\text{posture}}\dot{x}_{\text{posture}}\right) = 0, \tag{61}$$

which is asymptotically stable toward the minimum achievable energy as demonstrated in Sect. 5. To avoid tipping over because of quick jerks induced on the robot's center of mass, in the actual implementation, we add saturation policies to the above proportional-derivative controller. We saturate the maximum velocity and the maximum acceleration at which we allow the center of mass to move. The overall controller is depicted in Fig. 8.

In Fig. 9 we show a sequence of snapshots and accompanying data readings of one of the tests. The testing setup is identical to that depicted in Fig. 6 with varying slope angles formed by the boards. The robot starts on the flat terrain and as the human operator pulls the arm toward him, the robot enters the sloped portion of the terrain and climbs the sloped stretch. After moving approximately 1m upward, the human

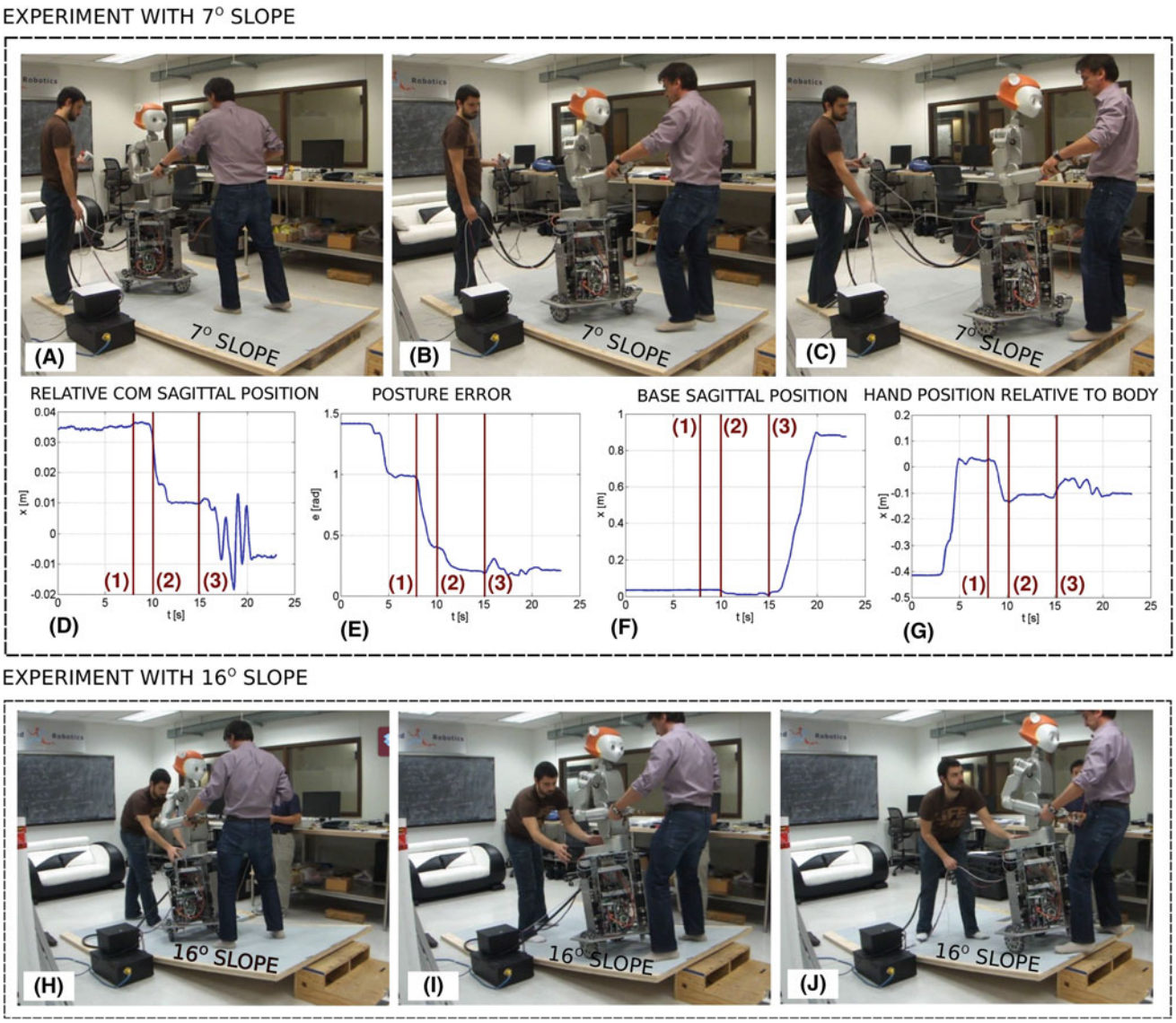

Fig. 9 *Tests on uneven terrain force interaction* Sequence of video snapshots, and data taken during the test on the irregular terrain. Snapshots, **a**–**c** correspond to maneuvers on a terrain of 7° slope. The corresponding data is shown on images (**d**)–(**g**). At instant (*1*) the upper body motors are enabled. At (*2*) the base motors are enabled. At (*3*) the robot starts ascending the slope. A second test was carried out with a slope of 16° shown in snapshots (**h**)–(**j**). The robot was able to handle the slope without falling but with great difficulty on keeping wheel traction

operator pushes the robot downward to the flat area. The human operator repeats the same movement three times. The speeds of the base moving in the terrain achieved a maximum of 0.35 m/s. We recorded data corresponding to the sequence of transitions between the flat to the sloped terrain going upward.

The graphic data corresponds to the test with the 7° slope. The first 8 seconds correspond to a period where the upper body and the base are not powered. The fluctuations of hand position and postural errors during this time are due to moving the upper arm. In the 8th second, the (initially engaged) emergency stop button of the upper body is released, which stabilizes the hand position and minimizes the postural error. The base has independent power and is turned on in the 10th second. Consequently, the center of mass relative error with respect to the center of the wheels is actively controlled at that time. The user waits a few seconds idle, and in the 15th second starts to pull the robot to climb the slope. As we can see, the base moves approximately 0.9m on the slope at a speed of about 0.35 m/s. During this time, the center of mass is kept within a relatively small error between the wheels to avoid falling down. The relative hand position also remains stable, close to the zero position error. Finally, the postural error is kept small in the task's null space throughout the interaction. A second test with a slope of 16° is also carried out and depicted on the bottom part of Fig. 9. No data

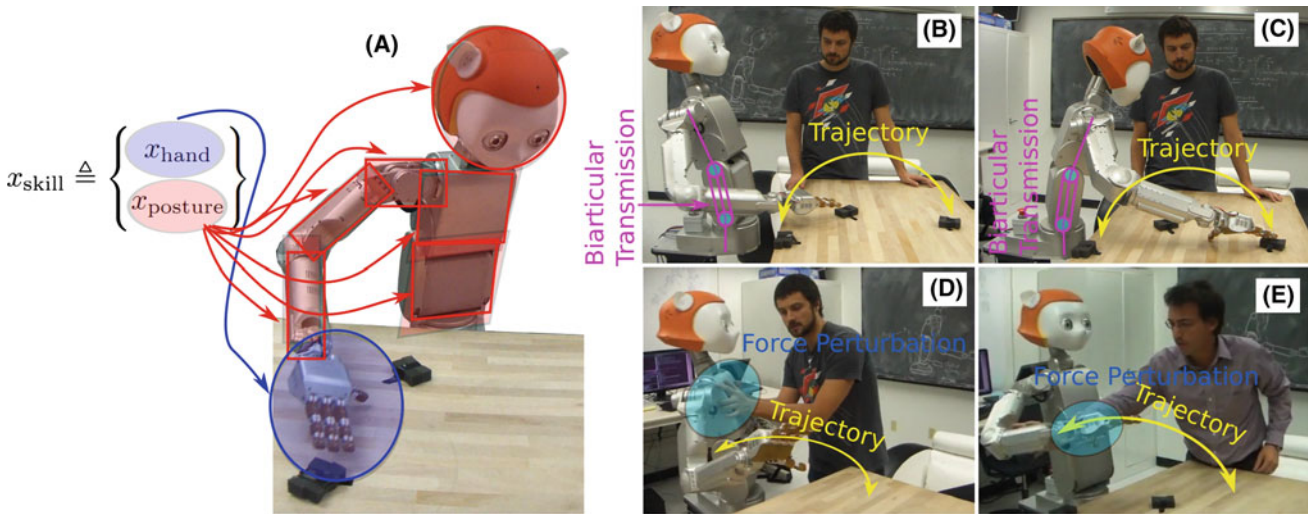

Fig. 10 *Tests on upper-body interactions and compliance* The interaction skill shown in **a** is created by aggregating the hand's Cartesian coordinate and a joint posture. The feedback control gains of both the task and the posture are chosen in the mid-range to respond compliantly to force perturbations. The hand is able to track the desired trajectory shown in (**b**) and (**c**). The posture error is equally distributed across all torso and arm joints to minimize the posture energy. All of this coordination is accomplished in spite of the presence of the biarticular transmission constraint. In **d** the torso is perturbed by the user while the hand attempts to track a trajectory. In **e** the forearm responds compliantly to the force perturbations of the user

was collected for this test. The robot was able to balance and follow the human, but the wheels did loose traction.

Another hardware test addressing compliant interactions of the upper body under biarticular constraints is carried out and shown in Fig. 10. The hand is commanded to touch various points on the table by following given trajectories. At the same time, users perturb the robot by shaking its upper body and its forearm. The robot responds compliantly to the disturbances and then resumes the tracking of the desired trajectories. Additionally, it was able to do so in spite of the presence of biarticular constraints on the body, demonstrating that those constraints are indeed accounted for in the model-based controllers. Different gains were used for the hand tracking task and the postural optimization. By reducing both gains, the robot was able to respond compliantly to user induced disturbances.

7 Discussion and conclusions

There are currently few run-time torque controllers for floating body humanoid robots tested in actual hardware. This paper presents an implementation of the Whole-Body Compliant Controllers described in Sentis (2007), (2010) on the Dreamer humanoid robot and operating in uneven terrains. Our controller runs at 200Hz on an Intel i3 CPU running Ubuntu 10.04 with the RTAI real-time kernel, which makes it sufficient for real-time feedback control applications. With efforts from many teams on implementing whole-body compliant control, there is a race to show the potential capabilities. Our implementation, provides better support for controlling the robot's residual redundancy by using postures and by extension of the same mechanism to resolve conflicts between tasks. Such built-in mechanism will provide effective support for sensor-based behaviors, because the controller can respond to the inherent conflict between task goals in a reactive manner.

There is a significant body of existing results and ongoing research in the community that investigates motion planning, optimization, and constrained control problems. However, for humanoid robots, the majority of the more advanced methods are still too slow to run at high frequencies. We are convinced, however, that whole-body control will inevitably need to combine optimization and motion planning techniques with the real-time control loops. The experiments we report in this paper are a first step in this direction. From a theoretical perspective, the main contribution of this paper is the proof of asymptotic stability of Sect. 5. Such control theoretic analysis is important to guarantee that the feedback and feedforward control processes of whole-body compliant control are stable and converge to the expected energy levels.

We have used models of Dreamer mostly derived from CAD models. We are aware that this decreases the accuracy of the control structures and causes model disturbances. We compensate for them by increasing the proportional gains, a technique often used in inverse kinematic controllers. Indeed, the latter lack a dynamic model to provide feedforward compensation. Limitations on gain values usually come from the rigidity of the robot and not from the modeling errors. In our case, because Dreamer has series elastic actuators,

proportional gains exceeding a moderate value of around 400 N/m can lead to instabilities. However, the experiment in Fig. 5 shows accurate performance of the upper body for moderate gains and for movements spanning a wide range of the workspace. We expect that tracking performance could be further improved via nonlinear methods such as Sliding Mode Control.

A source of error when balancing is due to estimation of the robot's center of mass. We have used the CAD models for that estimation and it has performed well because the base is relatively large. However, to have more accurate center of mass estimation one should use data-driven estimation procedures, such as the one suggested in Cotton et al. (2009). Moving the center of mass around is a delicate matter in humanoid robots. It is well known that the robot's center of pressure position is proportional to center of mass accelerations (Vukobratović and Borovac 2004). And for the type of terrains that we currently handle, the robot's center of pressure should remain approximately below the base's horizontal footprint to avoid tipping over. The robot being tall with a relatively slim base, an unexpected jerk can make the robot fall. One possible avenue for dealing with these constraints would be to obtain a model of the accelerations with respect to the center of pressure. This could be achieved via approximations, such as pendulum dynamics, or using a data-driven approach, to design center of mass trajectories that remain withing the base's footprint. In our hardware tests we chose instead to use a simple proportional-derivative control law with velocity and acceleration saturation for the center of mass. This ensures the absence of excessive jerks, but also limits the maximum frequency at which we can move the center of mass to about 3Hz for displacements of about 3cm.

The implementation on Dreamer of our Whole-Body Control algorithms, is hosted open-source on SourceForge with repositories on Github for both core generic libraries as well as the specific libraries for Dreamer. However, there is currently no technical support on those repositories. Also, the Whole-Body Control Framework is a joint framework developed by Stanford University and UT Austin.

At the application level, we have conducted hardware tests that show the capabilities of our control methods, with particular attention to sloped terrains. In particular, self-balancing allows Dreamer to climb slopes without falling. Currently, we are limited to sloped terrains that are smooth. This limitation is due to the construction of the omni wheels which have small rollers on the side that cannot overcome large obstacles. However, the presented algorithms could handle more difficult terrains, such as the ones encountered in city environments.

When maneuvering in steep slopes we have observed wheel slippage. The feedback controller minimizing the distance between the hand and the body causes the wheels to continuously rotate toward the direction where the hand is pushed to by the user. If the user pushes too hard, the robot's arm will approach singularity positions which could cause oscillations if unhandled. A future avenue of whole-body control will be to address these types of adversities in robust ways. Additionally, developing online estimation processes of the terrain properties would provide interesting insights in constraint characterization.

Future areas of research include developing a more rugged base capable of maneuvering in outdoor urban-like environments, incorporating torque sensor feedback on the base for better compliance, developing software interfaces to connect to high level planners, and developing motion planners for dynamic maneuvers in rough terrains. Another important area complementary to the research is to support the open source software by providing tutorials, mailing lists and updates for the new releases of the libraries used in our implementation.

Acknowledgments All experimental and hardware equipment were funded by the Mechanical Engineering Department at The University of Texas at Austin. The research was partly supported by a donation from Willow Garage to the University of Texas at Austin. The authors would like to thank Alan Kwok, Kwan Suk Kim and Nick Paine for their help during experimentation. The mobile base was built by Frank Lima, Somudro Gupta, and Pius Wong at The University of Texas at Austin. Technical support was provided by Meka Robotics. Figure 1 was provided by Ashish Deshpande.

Appendix

Derivations of prioritized whole-body compliant control based on previous work (Sentis et al. 2010)

Rigid multibody dynamics can be developed using the Lagrangian formalism, which leads to the following equation of motion,

$$A(q)\,\ddot{q} + b(q,\dot{q}) + g(q) + J_{\text{constr}}^{T}\,\lambda_{\text{constr}} = U^{T}\,\tau_{\text{control}}, \tag{62}$$

where $\{A, b, g\}$ are the inertial matrix, Coriolis-centrifugal, and gravity terms, $\tau_{\text{control}} \in \mathbb{R}^{n_{\text{dofs}}-(1+6)}$ is the vector of torques generated at the output of the motors (assuming completely rigid actuators), λ_{constr} are the Lagrangian multipliers associated with the tension forces on the biarticular transmission wire and the reaction forces on the wheel contacts against the ground. This Jacobian can be viewed as infinitesimal displacements of a coordinate δ_{constr} defined as

$$\dot{\delta}_{\text{constr}} \triangleq J_{\text{constr}}\,\dot{q} = 0. \tag{63}$$

Considering a rigid transmission in the biarticular joints and rigid contacts on the wheels, it is possible to obtain a model-based solution of the previous Lagrangian multipliers. By left multiplying Eq. (62) by $J_{\text{constr}}\,A^{-1}$, applying the time

derivatives of Eq. (63), i.e. $\ddot{\delta}_{\text{constr}} = J_{\text{constr}}\ddot{q} + \dot{J}_{\text{constr}}\dot{q} = 0$, the Lagrangian multipliers can be solved as

$$\lambda_{\text{constr}} = \overline{J}^{T}_{\text{constr}} \left(U^{T} \tau_{\text{control}} - b - g \right) + \Lambda_{\text{constr}} \dot{J}_{\text{constr}} \dot{q}, \tag{64}$$

where $\overline{J}_{\text{constr}} \triangleq A^{-1} J^{T}_{\text{constr}} \Lambda_{\text{constr}}$ is the dynamically consistent generalized inverse of (12) and $\Lambda_{\text{constr}} \triangleq (J_{\text{constr}} A^{-1} J^{T}_{\text{constr}})^{-1}$ is the joint inertial matrix projected into the manifold of the constraints.

Plugging the above Equation into (62) we remove the Lagrangian Multipliers term, yielding constrained dynamics

$$\begin{aligned} &A\ddot{q} + N^{T}_{\text{constr}} (b + g) + J^{T}_{\text{constr}} \Lambda_{\text{constr}} \dot{J}_{\text{constr}} \dot{q} \\ &\quad = (U N_{\text{constr}})^{T} \tau_{\text{control}}, \end{aligned} \tag{65}$$

where

$$N_{\text{constr}} \triangleq I - \overline{J}_{\text{constr}} J_{\text{constr}} \tag{66}$$

is the dynamically consistent null space of the constraint Jacobian.

It is of interest to formulate kinematic quantities in terms of actuated joints alone. In particular, we consider decomposing the generalized coordinates into actuated and floating / co-actuated portions, i.e.

$$q = D_{\text{kin}} \begin{pmatrix} q_{\text{act}} \\ q_{\text{unact}} \end{pmatrix}, \tag{67}$$

where D_{kin} is a matrix that distributes the joint coordinates of the actuated and floating / co-actuated joints to their respective positions in the robot's kinematic chain, q_{act} are the actuated joints (i.e. attached to a motor), and q_{unact} correspond to the floating and co-actuated degrees of freedom.

Because of condition (63), we can state that joint velocities lie in the null space of the constraints, i.e. $\dot{q}^{*} \in \text{Null}(J_{\text{constr}})$, where $\dot{q}^{*}$ expresses the set of generalized velocities that fulfills all of the constraints (see Sentis (2007) for details). In other words, the constrained velocities can be expressed as the self motion manifold $\dot{q}^{*} = (I - J^{\#}_{\text{constr}} J_{\text{constr}})\, \dot{q}$, where $J^{\#}_{\text{constr}}$ is any right inverse of the constraints Jacobian (i.e. $J_{\text{constr}} J^{\#}_{\text{constr}} = I$) and $\dot{q}$ represents unconstrained velocities.

The constrained generalized velocities can be reconstructed from the velocities of the actuated DoFs alone using the following formula

$$\dot{q}^{*} = \overline{UN}_{\text{constr}}\, \dot{q}_{\text{act}}, \tag{68}$$

where

$$\overline{UN}_{\text{constr}} \triangleq A^{-1} (U N_{\text{constr}})^{T} (\phi^{*})^{+}, \tag{69}$$

is the the dynamically consistent generalized inverse of UN_{constr}, $(.)^{+}$ is the Moore-Penrose pseudoinverse operator and

$$\phi^{*} \triangleq U N_{\text{constr}} A^{-1} (U N_{\text{constr}})^{T}, \tag{70}$$

is a projection of the inertia matrix in the reduced constrained manifold. Once more, see Sentis (2007) for a proof of (68).

Task entities to be controlled in the operational space can be expressed with a generic coordinate transformation $x_{\text{task}} = T_{\text{task}}(q) \in \mathbb{R}^{n_{\text{task}}}$, where T_{task} is a kinematic transformation matrix, e.g. a homogeneous transformation for a Cartesian point, or a rotation and translation in the group $SE(3)$ for a spatial transformation of a frame, n_{task} is the number of degrees of freedom of the task coordinates, and q is the generalized coordinates of the system including both the actuated and unactuated / co-actuated joints. It follows that instantaneous task kinematics can be expressed as $\dot{x}_{\text{task}} = J_{\text{task}}\, \dot{q}$, where $J_{\text{task}} = \partial x_{\text{task}} / \partial q \in \mathbb{R}^{n_{\text{task}} \times n_{\text{dofs}}}$ is the whole-body Jacobian matrix with respect to the generalized coordinates. The differential kinematics with respect to actuated joints alone can be expressed as

$$\dot{x}_{\text{task}} = J^{*}_{\text{task}}\, \dot{q}_{\text{act}}, \tag{71}$$

where J^{*}_{task} is the reduced constraint consistent Jacobian (a.k.a. Generalized Jacobian)

$$J^{*}_{\text{task}} \triangleq J_{\text{task}} \overline{UN}_{\text{constr}}, \tag{72}$$

with $J^{*}_{\text{task}} \in \mathbb{R}^{n_{\text{task}} \times n_{\text{act}}}$, being a reduced form of the task Jacobian consistent with the general constraint conditions, and n_{act} being the number of degrees of freedom of the actuated joints. To prove (71), consider the constrained generalized velocities $\dot{q}^{*}$, and apply (68) to the instantaneous task kinematics , thus getting $\dot{x}_{\text{task}} = J_{\text{task}} \dot{q}^{*} = J_{\text{task}} \overline{UN}_{\text{constr}}\, \dot{q}_{\text{act}}$.

Generalized Jacobians describe the relationship between instantaneous motions of the active hinges and the task frames. Additionally, they incorporate dynamic effects on the robot's motion, such as the conservation of momenta (Umetami and Yoshida 1989; Dubowsky and Papadopoulos 1993) and the contact dynamics (Sentis et al. 2010). In the context of our robot Dreamer, they are effective at deriving controllers for constrained underactuated / co-actuated systems since they define the behavior of robots with respect to the actuated joints alone.

Let us consider the skill of touching objects using Dreamer's right arm as shown in Fig. 10. We represent the skill using two coordinate systems,

$$x_{\text{skill}} \triangleq \begin{Bmatrix} x_{\text{hand}} \\ x_{\text{posture}} \end{Bmatrix}, \tag{73}$$

where $x_{\text{hand}} \in T(3)$ represents a coordinate attached to the hand midpoint, $T(3)$ is the group of translations and $x_{\text{posture}} = q_{\text{act}} \in \mathbb{R}^{n_{\text{act}}}$ is the vector of actuated joints. For instance, the posture might consist of minimizing the joint posture with respect to a static pose frame.

In general, a prioritized task coordinate, task(k), can be kinematically characterized by its Generalized constrained Jacobian which in a general sense it is constrained both by

the robot's physical constraints and by the higher priority tasks, i.e.

$$x_{\text{task}(k)} = T_{\text{task}(k)}(q), \tag{74}$$

$$\dot{x}_{\text{task}(k)} = J^*_{\text{task}(k)}\,\dot{q}_{\text{act}}, \tag{75}$$

where

$$J^*_{\text{task}(k)} \triangleq J_{\text{task}(k)}\overline{UN}_{\text{constr}}N^*_{\text{prec}(k)}, \tag{76}$$

and $N^*_{\text{prec}(k)}$ is the dynamically-consistent null-space of the higher priority tasks (i.e. preceding)

$$N^*_{\text{prec}(k)} \triangleq I - \sum_{i=1}^{k-1} \overline{J}^*_{\text{task}(i)} J^*_{\text{task}(i)}. \tag{77}$$

In the above derivations we have assumed that tasks with lower index k have higher priority. As such, the priorities are established by projecting lower priority tasks on the null space of preceding tasks.

It can be demonstrated Sentis (2007), that the dynamics of the actuated joints can be expressed as

$$\ddot{q}_{\text{act}} + \phi^*(b^* + g^*) = \phi^*\tau_{\text{control}}. \tag{78}$$

where

$$\phi^*(b^* + g^*) \triangleq UA^{-1}\left(N^T_{\text{constr}}(b+g) + J^T_{\text{constr}}\Lambda_{\text{constr}}\dot{J}_{\text{constr}}\dot{q}\right). \tag{79}$$

By left multiplying the above Equation by the generalized inverse

$$\overline{J}^*_{\text{task}(k)} \triangleq \phi^*\, J^{*T}_{\text{task}(k)}(J^*_{\text{task}(k)}\,\phi^*\,J^{*T}_{\text{task}(k)})^{-1}, \tag{80}$$

and using the equality defined by differentiating (75), i.e. $\ddot{x}_{\text{task}(k)} = J^*_{\text{task}(k)}\ddot{q}_{\text{act}} + \dot{J}^*_{\text{task}(k)}\dot{q}_{\text{act}}$, the constrained task dynamics can be expressed as

$$\Lambda^*_{\text{task}(k)}\ddot{x}_{\text{task}(k)} + \mu^*_{\text{task}(k)} + p^*_{\text{task}(k)} = \overline{J}^{*T}_{\text{task}(k)}\tau_{\text{control}}, \tag{81}$$

with $\{\Lambda^*_{\text{task}(k)}, \mu^*_{\text{task}(k)}, p^*_{\text{task}(k)}\}$ being inertial, Coriolis-centrifugal, and gravitational terms respectively and not derived here.

If $J^*_{\text{task}(k)}$ is full rank, the following control structure yields full control of the task's closed loop dynamics,

$$\tau_{\text{control}} = J^{*T}_{\text{task}(k)}F_{\text{task}(k)}. \tag{82}$$

This statement can be proven by plugging the above torques into Eq. (81) and using the property of the generalized inverse $J^*_{\text{task}(k)}\overline{J}^*_{\text{task}(k)} = I$, thus getting

$$\Lambda^*_{\text{task}(k)}\ddot{x}_{\text{task}(k)} + \mu^*_{\text{task}(k)} + p^*_{\text{task}(k)} = F_{\text{task}(k)}. \tag{83}$$

The above transformation can be used to provide full control of the task accelerations $\ddot{x}_{\text{task}(k)}$ whenever $\Lambda_{\text{task}}(k)$ is full rank. This is the case when there is no conflict between the k-th task and higher priority ones. By defining the control input as

$$F_{\text{task}(k)} = \Lambda^*_{\text{task}(k)}u_{\text{task}(k)} + \mu^*_{\text{task}(k)} + p^*_{\text{task}(k)}, \tag{84}$$

where $u_{\text{task}(k)}$ is an acceleration feedback control policy, the above controller yields closed loop dynamics

$$\ddot{x}_{\text{task}(k)} = u_{\text{task}(k)}. \tag{85}$$

In our scheme, tasks are coordinates that need to track a position or force trajectory or converge to a goal. In contrast, postures are objectives that need to optimize a performance criterion in the null space of tasks. As shown in Eq. (73), a skill has one or more task coordinates to be controlled and one or more postures to be optimized in the redundant space. For the case of one task and one posture, we define the following prioritized control structure,

$$\tau_{\text{control}} = J^{*T}_{\text{task}}F_{\text{task}} + N^{*T}_{\text{task}}\tau_{\text{posture}}, \tag{86}$$

where

$$N^*_{\text{task}} \triangleq I - \overline{J}^*_{\text{task}}J^*_{\text{task}}, \tag{87}$$

is the dynamically consistent null-space matrix of the reduced task Jacobian. An example of a three-priority controller is shown in Fig. 8.

References

Aghili, F. (2005). A unified approach for inverse and direct dynamics of constrained multibody systems based on linear projection operator: applications to control and simulation. *IEEE Transactions on Robotics*, *21*(5), 834–849.

Alami, R., Chatila, R., Fleury, S., Ghallab, M., & Ingrand, F. (1998). An architecture for autonomy. *The International Journal of Robotics Research*, *17*(4), 315–337.

Arkin, R. C., & Murphy, R. R. (1990). Autonomous navigation in a manufacturing environment. *IEEE Transactions on Robotics and Automation*, *6*(4), 445–454.

Asfour, T., Berns, K., & Dillmann, R. (2000). *The humanoid robot armar: Design and control. The 1st IEEE-ras international conference on humanoid robots (humanoids 2000)* (pp. 7–8).

Babic, J. (2009). *Biarticular legged robot: Design and experiments. IEEE international conference on robotics and biomimetics*. Bankok, Thailand.

Baerlocher, P. (2001). *Inverse kinematics techniques for the interactive posture control of articulated figures*. Ph.D. thesis, Ecole Polytechnique Federale de Lausanne, Lausanne, Switzerland.

Beetz, M., Mo, L., Senlechner, & Tenorth, M. (2010). *A cognitive robot abstract machine for everyday manipulation in human environments. IEEE/rsj international conference on Intelligent robots and systems (iros)* (pp. 1012–1017).

Bouyarmane, K., & Kheddar, A. (2011). *Multi-contact stances planning for multiple agents. Proceedings of the IEEE international conference on robotics and automation*. Shanghai.

Breazeal, C., Siegel, M., Berlin, M., Gray, J., Grupen, R., Deegan, P., Weber, J., Narendran, K., & McBean, J. (2008). Mobile, dexterous, social robots for mobile manipulation and human-robot interaction. SIGGRAPH08: ACM SIGGRAPH 2008 new tech demos.

Brock, O., Khatib, O., & Viji, S. (2002). *Task-consistent obstacle avoidance and motion behavior for mobile manipulation. Proceedings of the ieee international conference on robotics and automation* (pp. 388–393). Washingtion, USA.

Chang, K. S., Holmberg, R., & Khatib, O. (2000). The augmented object model: Cooperative manipulation and parallel mechanism dynamics. *Proceedings of IEEE international conference on robotics and automation*, *1*, 470–475.

Cotton, S., Murray, A. P., & Fraisse, P. (2009). Estimation of the center of mass: From humanoid robots to human beings. *IEEE/ASME Transactions on Mechatronics*, *14*(6), 707–712.

DeLuca, A. (1991). Zero dynamics in robotics systems. *Proceedings of the IIASA Workshop Progress in Systems and Control Theory*, *9*, 70–87.

Dietrich, A., Wimbock, T. & Albu-Schaffer, A. (2011). *Dynamic whole-body mobile manipulation with a torque controlled humanoid robot via impedance control laws. IEEE/rsj international conference on Intelligent robots and systems (iros)* (pp. 3199–3206).

Dubowsky, S., & Papadopoulos, E. (1993). he kinematics, dynamics, and control of free-flying and free-floating space robotic systems. *IEEE Transactions on Robotics and Automation*, *9*(5), 531–543.

Edsinger, A., & Kemp, C. (2008). Two arms are better than one: A behavior based control system for assistive bimanual manipulation. *Recent progress in robotics: Viable robotic service to human*.

Featherstone, R. (1987). *Robot dynamics algorithms*. Norwell, USA: Kluwer Academic Publishers.

Freitas, G., Lizarralde, F., Hsu, L., & Reis, N., Salvi dos R. (2009). *Kinematic reconfigurability of mobile robots on irregular terrains. IEEE international conference on robotics and automation (ICRA)* (pp. 1340–1345).

Fuchs, M., Borst, C., Giordano, P. R., Baumann, A., Kraemer, E., Langwald, J., Gruber, R., Seitz, N., Plank, G., Kunze, K., Burger, R., Schmidt, F., Wimboeck, T., & Hirzinger, G. (2009). *Rollin' justin: Design considerations and realization of a mobile platform for a humanoid upper body. IEEE international conference on robotics and automation (ICRA)*, (pp. 4131–4137).

Halme, A., Leppänen, I., & Salmi, S. (1999). *Development of workpartner-robot-design of actuating and motion control system. 2nd international conference on climbing and walking robots, portsmouth* (pp. 657–666).

Hanafusa, H., Yoshikawa, T., & Nakamura, Y. (1981). *Analysis and control of articulated robot with redundancy. Proceedings of IFAC symposium on robot control*. Vol. 4, (pp. 1927–1932).

Hart, S., Yamokoski, J. D., & Diftler, M. (2011). Robonaut 2: A new platform for human-centered robot learning. Robotics Science and Systems.

Hirose, S., et al. (1991). *Design of practical snake vehicle: Articulated body mobile robot kr-2. The 5th international conference on advanced robotics*, (pp. 833–838).

Holmberg, R., & Khatib, O. (2000). Development and control of a holonomic mobile robot for mobile manipulation tasks. *The International Journal of Robotics Research*, *19*(11), 1066–1074.

Hyon, S.-H., Hale, J., & Cheng, G. (2007). Full-body compliant human-humanoid interaction: Balancing in the presence of unknown external forces. *IEEE Transactions on Robotics*, *23*(5), 884–898.

Iwata, H., & Sugano, S. (2009). *Design of human symbiotic robot twendy-one. IEEE international conference on robotics and automation (ICRA)* (pp. 580–586).

Jenkins, O. C., & Mataric, M. J. (2004). Performance-derived behavior vocabularies: Data-driven acqusition of skills from motion. *International Journal of Humanoid Robotics*, *1*(2), 237–288.

Katz, D., Horrell, E., Yang, Y., Burns, B., Buckley, T., Grishkan, A., Zhylkovskyy, V., Brock, O., & Learned-Miller, E. (2006). The umass mobile manipulator uman: An experimental platform for autonomous mobile manipulation. Workshop on manipulation in human environments at robotics: Science and systems.

Khatib, O. (1987). A unified approach for motion and force control of robot manipulators: The operational space formulation. *International Journal of Robotics Research*, *3*(1), 43–53.

Khatib, O., Sentis, L., Park, J. H., & Warren, J. (2004). Whole body dynamic behavior and control of human-like robots. *International Journal of Humanoid Robotics*, *1*(1), 29–43.

Kim, K.-G., Lee, J.-Y., Choi, D., Park, J.-M. & You, B.-J. (2010). *Autonomous task execution of a humanoid robot using a cognitive model. IEEE international conference on robotics and biomimetics (ROBIO)*, (pp. 405–410).

Kimura, N., et al. (1991). *Locomotion mechanism and its control architecture for disaster preventing robot. Proceedings of international symposium on advanced robot technology*, (pp. 375–380).

King, C.-H., Chen, T. L., Jain, A., & Kemp, C. C. (2010). *Towards an assistive robot that autonomously performs bed baths for patient hygiene. IEEE/rsj international conference on intelligent robots and systems (IROS)*, (pp. 319–324).

Lengagne, S., Vaillant, J., Yoshida, E., & Kheddar, A. (2013). Generation of whole-body optimal dynamic multi-contact motions. *The International Journal of Robotics Research*.

Matsumoto, O., Kajita, S., Tani, K., & Oooto, M. (1995). A four-wheeled robot to pass over steps by changing running control modes. IEEE international conference on robotics and automation. Vol. 2, (pp. 1700–1706).

Meeussen, W., Wise, M., Glaser, S., Chitta, S., McGann, C., Mihelich, P., Marder-Eppstein, E., Muja, M., Eruhimov, V., Foote, T., Hsu, J., Rusu, R.B., Marthi, B., Bradski, G., Konolige, K., Gerkey, B., & Berger, E. (2010). *Autonomous door opening and plugging in with a personal robot. IEEE international conference on robotics and automation (ICRA)*, (pp. 729–736).

Mistry, M., Buchli, J., & Schaal, S. (2010). *Inverse dynamics control of floating base systems using orthogonal decomposition. Proceedings of the IEEE international conference on robotics and automation*, (pp. 3406–3412).

Mistry, M., and Righetti, L. (2011). Operational space control of constrained and underactuated systems. Robotics: Science and systems VII.

Nagasaka, K., Kawanami, Y. Shimizu, S., Kito, T., Tsuboi, T., Miyamoto, A., Fukushima, T., & Shimomura, H. (2010). *Whole-body cooperative force control for a two-armed and two-wheeled mobile robot using generalized inverse dynamics and idealized joint units. IEEE international conference on robotics and automation (ICRA)*, (pp. 3377–3383).

Nakamura, Y., Hanafusa, H., & Yoshikawa, T. (1987). Task-priority based control of robot manipulators. *International Journal of Robotics Research*, *6*(2), 3–15.

Nakanishi, J., Mistry, M., & Schaal, S., (2007). *Inverse dynamics control with floating base and constraints. IEEE international conference on robotics and automation*, pp. 1942–1947.

Nakano, E., & Nagasaka, S. (1993). *Leg-wheel robot: A futuristic mobile platform for forestry industry. Proceedings of IEEE/Tsukuba international workshop on advanced robotics*, (pp. 109–112).

Oh, S., Kimura, Y., & Hori, Y. (2010). *Force control based on biarticular muscle system and its application to novel robot arm driven by planetary gear system. IEEE/rsj international conference on intelligent robots and systems*, Taipei.

Ohmichi, T., et al. (1985). *Development of the multi-function robot for the containment vessel of the nuclear plant. Proceedings of international conference on advanced robotics*, (pp. 371–378).

Oriolo, G., (1994). *Stabilization of self-motions in redundant robots. Proceedings IEEE international conference on robotics and automation*, (pp. 704–709).

Pastor, P., Hoffmann, H., Asfour, T. & Schaal, S. (2009). *Learning and generalization of motor skills by learning from demonstration. IEEE international conference on robotics and automation (ICRA)*, (pp. 763–768).

Philippsen, R., Sentis, L., & Khatib, O. (2011). *An open source extensible software package to create whole-body compliant skills in personal mobile manipulators. IEEE/rsj international conference on intelligent robots and systems (IROS)*, (pp. 1036–1041).

Reiser, U., Connette, C., Fischer, J., Kubacki, J., Bubeck, A., Weisshardt, F., Jacobs, T., Parlitz, C., Hagele, M., & Verl, A. (2009). *Care-o-bot; 3: Creating a product vision for service robot applications by integrating design and technology. IEEE/rsj international conference on intelligent robots and systems (IROS)*, (pp.1992–1998).

Righetti, L., Buchli, J., Mistry, M., & Schaal, S. (2011). *Inverse dynamics control of floating-base robots with external constraints: A unified view. IEEE international conference on robotics and automation (ICRA)*, (pp. 1085–1090).

Righetti, L., Buchli, J., Mistry, M., Kalakrishnan, M., & Schaal, S. (2013). Optimal distribution of contact forces with inverse dynamics control. *The International Journal of Robotics Research*, *32*(3), 280–298.

Saab, L., Ramos, O. E., Keith, F., Mansard, N., Soueres, P., & Fourquet, J.-Y. (2013). Dynamic whole-body motion generation under rigid contacts and other unilateral constraints.

Salini, J. (2012). *Dynamic control for the task/posture coordination of humanoids: Toward synthesis of complex activities. These de doctorat*. Paris, France: Universit Pierre et Marie Curie.

Salini, J., Padois, V., Ibanez, A., Bidaud, P., & Buendia, A. (2011). *A goal driven perspective to generate humanoid motion synthesis. Field robotics: Proceedings of the 14th international conference on climbing and walking robots and the support technologies for mobile machines*, (pp. 889–897). World Scientific.

Schaal, S., Auke, I., & Aude, B. (2003). Computational approaches to motor learning by imitation. *Philosophical Transactions of the Royal Society of London. Series B: Biological Sciences*, *358*(1413), 537–547.

Sentis, L. (2007). Synthesis and control of whole-body behaviors in humanoid systems. Ph.D. thesis, Stanford University, Stanford, USA.

Sentis, L., & Khatib, O. (2005). Synthesis of whole-body behaviors through hierarchical control of behavioral primitives. *International Journal of Humanoid Robotics*, *2*(4), 505–518.

Sentis, L., Park, J., & Khatib, O. (2010). Compliant control of multicontact and center of mass behaviors in humanoid robots. *IEEE Transactions on Robotics*, *26*(3), 483–501.

Sentis, L., Petersen, J., & Philippsen, R. (2012). Experiments with balancing on irregular terrains using the dreamer mobile humanoid robot. Robotics science and systems, Sidney.

Siciliano, B., & Slotine, J., (1991). *A general framework for managing multiple tasks in highly redundant robotic systems. Proceedings of the IEEE international conference on advanced robotics*, (pp. 1211–1216). Pisa, Italy

Simmons, R., & Apfelbaum, D. (1998). *A task description language for robot control. Proceedings IEEE/rsj international conference on Intelligent robots and systems*, Vol. 3, (pp. 1931–19373).

Stilman, M., Olson, J., Gloss, W. (2010). Golem krang: Dynamically stable humanoid robot for mobile manipulation. IEEE international conference on robotics and automation (ICRA), (pp. 3304–3309).

Theobold, D., Ornstein, J., Nichol, J. G., Kullberg, S. E., et al. (2008). Mobile robot platform Google Patents. US Patent 7,348,747.

Umetami, Y., & Yoshida, K. (1989). Resolved motion rate control of space manipulators with generalized Jacobian matrix. *IEEE Transactions on Robotics and Automation*, *5*(3), 303–314.

Vallery, H., Ekkelenkamp, R., Van Der Herman, K., & Buss, M. (2007). *Passive and accurate torque control of series elastic actuators. IEEE/rsj international conference on intelligent robots and systems (IROS)*, (pp. 3534–3538).

Volpe, R., Nesnas, I., Estlin, T., Mutz, D., Petras, R., & Das, H. (2001). The claraty architecture for robotic autonomy. IEEE proceedings on aerospace conference, Vol. 1, (pp. 1–12111321).

Vukobratović, M., & Borovac, B. (2004). Zero-moment point thirty tive years of its life. *International Journal of Humanoid Robotics*, *1*(1), 157–173.

Wakita, K., Huang, J., Di, P., Sekiyama, K., & Fukuda, T. (2011). Human-walking-intention-based motion control of an omnidirectional-type cane robot. *IEEE/ASME Transactions on Mechatronics*, *99*, 1–12.

Wilcox, B. H., Litwin, T., Biesiadecki, J., Matthews, J., Heverly, M., Morrison, J., et al. (2007). Athlete: A cargo handling and manipulation robot for the moon. *Journal of Field Robotics*, *24*(5), 421–434.

Ylonen, S. J., & Halme, A. J. (2002). *Workpartner: centaur like service robot. IEEE/rsj international conference on intelligent robots and systems* Vol. 1, (pp. 727–732).

Luis Sentis is an Assistant Professor in the University of Texas at Austin where he directs the Human Centered Robotics Laboratory. His research focuses on foundations for the compliant control of humanoid robots, algorithms to generate extreme dynamic locomotion, and building robots for educating students in mechatronics. He holds Ph.D. and MS degrees in Electrical Engineering from Stanford University where he developed leading work in theoretical and computational methods for the compliant control of humanoid robots. Prior to that, he worked in Silicon Valley in the area of clean room automation.

Josh Petersen received the B.Sc. degree in Mechanical Engineering from Cornell University in 2009 and the M.S. in Mechanical Engineering from Stanford University in 2011. He is currently a research assistant at UT Austin in the Human Centered Robotics Lab working on the Dreamer robot and doing research on physical human robot interaction and control of mobile robots in rough terrains.

Roland Philippsen I received my Ph.D. from EPFL, Switzerland, in 2005, for work on mobile robot path planning and obstacle avoidance. My expertise lies in interweaving reasoning, planning, and control. My current research interest lies in robots that take an active part in modifying their environment, while also pursuing applied research in intelligent vehicles with industrial partners. Some of the real-world robotics project I have contributed to are: tour-guide robots at the Swiss Expo.02, educational robots for the EPFL student contest 2001–2004, robotic actors for a theater play in 2005, a Cognitive Robot Companion in 2006, the PR2 of Willow Garage Inc, and the Meka robot of HCRL at UT Austin. I always try to push for robust open source software in this area, because I believe that autonomous robots can improve the lives of all humanity, provided we openly share knowledge and implementations.